NUMERICAL SIMULATION OF THE DRIFT-SCALE HEATER TEST AT YUCCA MOUNTAIN: SEPTEMBER 2002 STATUS REPORT

Prepared for

U.S. Nuclear Regulatory Commission
Contract NRC–02–02–012

Prepared by

Ronald T. Green
Scott L. Painter

Center for Nuclear Waste Regulatory Analyses
San Antonio, Texas

September 2007

ABSTRACT

This report documents the Center for Nuclear Waste Regulatory Analyses (CNWRA) thermal-hydrological modeling analysis of the Drift-Scale Heater Test to predict the temperature and saturation distribution in the rock during the heating and cooling phases of the test. The outcome of these predictive analyses is compared with temperatures measured during 4 years of heating. The multiphase code MULTIFLO (Painter, et al., 2001) was used in all simulations. Saturation measurements from the Drift-Scale Heater Test were not sufficiently unambiguous to allow quantitative comparison with model results. Nonetheless, the effect of alternatives to the conceptual models are evaluated in terms of predicted saturation in addition to temperature.

The basis for the conceptual and numerical models used in these analyses is presented in this report. Modeling results of the Drift-Scale Heater Test reported here build on previous CNWRA results (Green, et al., 2000, 2001). The Drift-Scale Heater Test model was enhanced by expanding it from two to three dimensions, invoking an improved active fracture model, including conductive and radiative heat loss through the bulkhead, and assigning more representative boundary conditions to the drift wall. Analyses conducted as part of this study evaluated the effects of alternative conceptual models and key property value assignments on model predictions. An alternative conceptual model that incorporated an active fracture model (Liu, et al., 1998) and fracture gas permeability represented with a Brooks-Corey relationship had an indistinguishable effect during the heating phase, but did affect calculation of the ambient matrix saturation. The assignment of block size {i.e., either 0.4 [1.3] or 5.0 m [16.4 ft]} was found to affect both ambient matrix saturation and heat and mass transfer in the presence of heating. A block size of 0.4 m [1.3 ft] provided better agreement with measured temperatures. The effect of heat and mass loss through the heated drift bulkhead was assessed. Mass loss as water vapor out of the heated drift was accommodated with the enhanced drift wall boundary condition. Heat loss out of the heated drift by conduction and radiation was incorporated by reducing the canister heat load (applied uniformly per unit surface area to the drift wall) by 20 percent. Differences in temperatures measured at the drift wall indicate that uniformly applying the canister heat load to the drift wall results in heat loadings that are not representative of those experienced at the Drift-Scale Heater Test.

Thermal-hydrological modeling results will be used subsequently to perform thermal-hydrological-mechanical analyses. These modeling studies are an important part of assessing and developing confidence in both the U.S. Department of Energy models and those developed on behalf of the U.S. Nuclear Regulatory Commission to independently evaluate a license application for a potential geologic repository at Yucca Mountain.

Technical Agreements TEF.2.01, TEF.2.08, TEF.2.10, and TEF.2.11 were addressed in this study. The effect of heat and mass loss through the bulkhead during the Drift-Scale Heater Test (TEF.2.01) was analyzed using an enhanced numerical model of the Drift-Scale Heater Test. Disagreement between measured and predicted temperatures near the drift wall suggests that heat loss through the bulkhead is not completely represented by the manner in which the canister heat load was applied to the model and the method used to represent conductive and radiative heat loss through the bulkhead. Penetration of the boiling isotherm by water refluxing down fractures, as represented by the O.M. Phillips analytical solution (Phillips, 1996), (TEF.2.08) was not directly addressed in these analyses. Nonetheless, accurate prediction of the extent of drying and the formation of heat pipes in partially saturated fractured rock in the presence of heating is imperative if the refluxing phenomenon is to be adequately understood

and predicted. The effect of variability of select thermodynamic variables on heat and mass transfer was assessed (TEF.2.11). Thermodynamic variables investigated in this study were matrix/fracture interaction properties, thermal conductivity properties assigned to the wing heater boreholes and the drift wall, and block dimensions. These properties were investigated because of their potentially significant impact on heat and mass transfer in fractured rock. Property values used in this enhanced thermodynamic model were taken from the most current listing of calibrated properties (TEF.2.11) (CRWMS M&O, 2001).

References

CRWMS M&O. "Multiscale Thermohydrologic Model." ANL–EBS–MD–000049. Rev. 00 ICN 02. North Las Vegas, Nevada: CRWMS M&O. 2001.

Green, R.T., M.E. Hill, and S. Painter. "Progress Report for DECOVALEX III Task 2: Numerical Simulation of the Drift-Scale Heater Test at Yucca Mountain." San Antonio, Texas: CNWRA. 2001.

Green, R.T., D. Hughson, S. Painter, and M.E. Hill. "Evaluation of the Drift-Scale Heater Test Thermal-Hydrological Conceptual Model Data and U.S. Department of Energy Thermal Test Results—Status Report." San Antonio, Texas: CNWRA. 2000.

Liu, H.H., C. Doughty, and G.S. Bodvarsson. "An Active Fracture Model for Unsaturated Flow and Transport in Fractured Rock." *Water Resources Research*. Vol. 34, No. 10. pp. 2,633–2,646. 1998.

Painter, S.L., Lichtner, P.C., and M.S. Seth. "MULTIFLO User's Manual: Two-Phase Nonisothermal Coupled Thermal-Hydrologic-Chemical Flow Simulator." MULTIFLO Version 1.5. San Antonio, Texas: CNWRA. 2001.

Phillips, O.M. "Infiltration of a Liquid Finger Down a Fracture into Superheated Rock." *Water Resources Research*. Vol. 32, No. 6. pp. 1,665–1,670. 1996.

CONTENTS

FIGURES

TABLES

ACKNOWLEDGMENTS

This report was prepared to document work performed by the Center for Nuclear Waste Regulatory Analyses (CNWRA) for the U.S. Nuclear Regulatory Commission (NRC) under Contract No. NRC–02–02–012. The activities reported here were performed on behalf of the NRC Office of Nuclear Material Safety and Safeguards, Division of High-Level Waste Repository Safety. The report is an independent product of the CNWRA and does not necessarily reflect the views or regulatory position of the NRC.

The authors thank R. Fedors and B. Sagar for technical and programmatic reviews of this document. The authors are thankful to P. Houston for typing the report and to C. Cudd, B. Long, and A. Woods for providing a full range of editorial services in preparation of the final document. The authors also thank M. Seth for assistance in assessing applications of the MULTIFLO code.

This report was originally delivered to NRC in September 2002. In September 2007, several minor programmatic changes were made in the text. It should be noted that Technical Agreements TEF.2.01 and TEF.2.08 were open at the time this report was delivered to U.S. NRC in September 2002, but were closed at the time this report was released in September 2007. These programmatic changes do not affect the technical information presented herein.

QUALITY OF DATA, ANALYSES, AND CODE DEVELOPMENT

DATA: No CNWRA-generated original data are contained in this report.

ANALYSES AND CODES: MULTIFLO code Version 1.5.1 software developed according to CNWRA quality assurance procedures was used in all analyses reported in this document.

1 INTRODUCTION

1.1 Background

The U.S. Department of Energy (DOE) is conducting a long-term, large-scale, *in situ* thermal Drift-Scale Heater Test in the Exploratory Studies Facility at Yucca Mountain, Nevada, to support its high-level waste program. The Drift-Scale Heater Test is part of an overall thermal testing strategy by DOE to gain a more indepth understanding of the heat-driven processes in the rock surrounding a potential high-level waste repository at Yucca Mountain. The overall objective of the Drift-Scale Heater Test is to acquire a more indepth understanding of coupled thermal, mechanical, hydrological, and chemical processes that will occur in the rock surrounding the emplaced high-level waste. The Drift-Scale Heater Test was designed to have a 4-year heating phase followed by a 4-year cooling phase. The heating phase started on December 3, 1997, and concluded on January 14, 2002.

An understanding of coupled processes is essential for assessment of the long-term performance of a potential high-level waste repository. Performance of the repository will be assessed using numerical simulations based on conceptual and mathematical models. The U.S. Nuclear Regulatory Commission (NRC), with assistance from the Center for Nuclear Waste Regulatory Analyses (CNWRA), is responsible for reviewing the DOE performance assessments. A three-dimensional numerical model was constructed by the CNWRA to evaluate the conceptual models and property value assignments used by DOE to simulate coupled thermohydrological processes observed during the Drift-Scale Heater Test.

1.2 Objective

This study evaluates the DOE conceptual models and characterization of the Drift-Scale Heater Test. Results from the analyses will assist NRC in assessing of the DOE and NRC technical agreements. Five technical agreement assessments directly benefit from the analyses reported in this document:

- TEF.2.01: “Consider measuring losses of mass and energy through the bulkhead of the Drift-Scale Heater Test and provide the technical basis for any decision or method decided upon (include the intended use of the results of the Drift-Scale Heater Test such as verifying assumptions in FEP exclusion arguments or providing support for TSPA models. The DOE should analyze uncertainty in the fate of thermally mobilized water in the Drift-Scale Heater Test and evaluate the effect this uncertainty has on conclusions drawn from the Drift-Scale Heater Test results. The DOE position is that measuring mass and energy losses through the bulkhead of the Drift-Scale Heater Test is not necessary for the intended use of the Drift-Scale Heater Test results. The Drift-Scale Heater Test results are intended for validation of models of thermally-driven coupled processes in the rock, and measurements are not directly incorporated into TSPA models. Results of the last two years of data support the validation of Drift-Scale Heater Test coupled-process models and the current treatment of mass and energy loss through the bulkhead. The DOE will provide the NRC a white paper on the technical basis for the DOE’s understanding of heat and mass losses through the bulkhead and their effects on the results by April 2001. This white paper will include the DOE’s technical basis for its decision regarding measurements of heat and mass losses

through the Drift-Scale Heater Test bulkhead. This white paper will address uncertainty in the fate of thermally mobilized water in the Drift-Scale Heater Test and also the effect this uncertainty has on conclusions drawn from the Drift-Scale Heater Test results. The NRC will provide comments on this white paper. The DOE will provide analyses of the effects of this uncertainty on the uses of the Drift-Scale Heater Test in response to NRC comments."

- TEF.2.08: "Provide the Mountain Scale Coupled Processes AMR, or any other appropriate AMR, documenting the results of the outlined items on page 20 of the OI 7 presentation (considering the NRC suggestion to compare model results to the O.M. Phillips analytical solution documented in Water Resources Research, 1996). The DOE will provide the updated Mountain-Scale Coupled Processes Model AMR (MDL–NBS–HS–000007) Rev 01 to the NRC in FY 02, documenting the results of the outlined items on page 20 of DOE's Open Item 7 presentation at this meeting. The DOE will consider the NRC suggestion of comparing the numerical model results to the O.M. Phillips analytical solution documented in WRR (1996)."

- TEF.2.10: "Represent the full variability/uncertainty in the results of the TEF simulations in the abstraction of thermodynamic variables to other models, or provide technical basis that a reduced representation is appropriate (considering risk significance). The DOE will discuss this issue during the TSPAI technical exchange tentatively scheduled for April 2001."

- TEF.2.11: "Provide the Calibrated Properties AMR, incorporating uncertainty from all significant sources. The DOE will provide an updated Calibrated Properties Model AMR (MDL–NBS–HS–000003) Rev 01 that incorporates uncertainty from significant sources to the NRC in FY 02."

- TEF.2.12: "Provide the Unsaturated Zone Flow and Transport PMR, Rev. 00, ICN 02, documenting the resolution of issues on page 5 of the OI 8 presentation. The DOE will provide the Unsaturated Zone Flow and Transport PMR (TDR–NBS–HS–000002) Rev 00 ICN 02 to the NRC in February 2001. It should be noted, however, that not all of the items listed on page 5 of the DOE's Open Item 8 presentation at this meeting are included in that revision. The DOE will include all the items listed on page 5 of the DOE's Open Item 8 presentation in Revision 02 of the Unsaturated Zone Flow and Transport PMR, scheduled to be available in FY 02."

Technical Agreements TEF.2.01, TEF.2.08, TEF.2.10, TEF.2.11, and TEF.2.12 are all currently open.[1]

1.3 Scope

A three-dimensional numerical model was assembled and run to perform the analyses of the DOE coupled thermohydrological models. MULTIFLO Version 1.5.1 (Painter, et al., 2001) was used to perform the simulations. The DOE property values and initial and boundary conditions

[1]Technical agreements TEF.2.01 and TEF.2.08 were open at the time this report was delivered to U.S. NRC in September 2002, but were closed at the time this report was released in September 2007.

were evaluated in these analyses. Conceptual models for dual continua and the active fracture model (Liu, et al., 1998) were also evaluated. Temperatures measured during the 4-year heating phase of the Drift-Scale Heater Test were used as the basis for the evaluations. The current status of these evaluations is reported in this document. The topics addressed in this report are (i) justification and definition of the mathematical model used in the thermohydrological analyses, (ii) justification of the values adopted for the parameters defining the mathematical model, (iii) numerical solution of the mathematical model, (iv) numerical simulation of the heating phase of the Drift-Scale Heater Test, and (v) comparison of modeling results with measured Drift-Scale Heater Test temperatures. These modeling studies are an important part of the process of assessing and developing confidence in both the DOE models and those developed on behalf of NRC to independently evaluate the safety case for a potential geologic repository at Yucca Mountain.

2 MATHEMATICAL SETTING

The MULTIFLO code Version 1.5.1 was used in the analyses reported in this document (Painter, et al., 2001). MULTIFLO is a general code for simulating multiphase, multicomponent, transport processes in nonisothermal systems with chemical reactions and reversible and irreversible phase changes in solids, liquids, and gases. Portions of the following description of MULTIFLO are taken from Painter, et al. (2001). Additional descriptions of flux terms between the matrix and fracture continua and of the active fracture model have been added here because of their importance in the analysis of the Drift-Scale Heater Test.

The MULTIFLO code consists of two sequentially coupled submodules: Mass and Energy TRAnsport (METRA) and General Electrochemical Migration (GEM). METRA solves mass balance equations for water and air and an energy balance equation. GEM solves mass balance equations for multicomponent reactive transport of solute species. Only transport of air, water, and heat was simulated in these analyses; therefore, only the METRA submodule was used in these analyses. Chemical transport at the Drift-Scale Heater Test is not investigated as part of these analyses.

METRA represents multiphase flow through three dimensions, although zero, one, or two dimensions are also possible. Single-phase (i.e., all liquid or all gas) or two-phase systems can be simulated. The equation of state for water in METRA allows temperatures in the 1–800 °C [33.8–1,472 °F] range and pressures below 165 bars. A description of the mathematical basis for METRA is presented in this chapter. A discussion of the balance equations is followed by the constitutive equations and the dual continuum model formulation.

2.1 Conservation Equations

The conservation equation for the water component (*w*) is given by

$$\frac{\partial}{\partial t}\left[\varphi\left(s_l n_l X_w^l + s_g n_g X_w^g\right)\right] + \nabla\cdot\left(q_l n_l X_w^l + q_g n_g X_w^g - D_g^{\text{eff}} n_g \nabla X_w^g\right) = Q_w \qquad (2\text{-}1)$$

and for the air component (*a*) by

$$\frac{\partial}{\partial t}\left[\varphi\left(s_l n_l X_a^l + s_g n_g X_a^g\right)\right] + \nabla\cdot\left(q_l n_l X_a^l + q_g n_g X_a^g - D_g^{\text{eff}} n_g \nabla X_a^g\right) = Q_a \qquad (2\text{-}2)$$

with source terms Q_w and Q_a, and where ∇ denotes gradient and φ is porosity. Subscripts and superscripts *g* and *l* denote the gas and liquid phases. In these equations, mass transport, q_l and q_g, is represented by Darcy's Law (as modified by the relative permeability for multiphase flow), which includes capillarity, gravity, and viscous forces

$$q_l = -\frac{k k_{rl}}{\mu_l}\nabla\left(P_l - \rho_l g z\right) \qquad (2\text{-}3)$$

and

$$q_g = -\frac{kk_{rg}}{\mu_g}\nabla\left(P_g - \rho_g g z\right) \tag{2-4}$$

where k denotes permeability, $k_{rl,rg}$ the relative permeability, $P_{l,g}$ the fluid pressure, $\mu_{l,g}$ the viscosity with mass densities $\rho_{l,g}$, g is the acceleration of gravity, *and* z is the vertical dimension. The densities of the liquid and gas phases based on a molar representation are represented by $n_{l,g}$. Gas mixture properties are calculated assuming the ideal gas law. Gas viscosity is calculated using the kinetic theory of gases (Hirschfelder, et al., 1954). The mole fractions $X_w^{l,g}$ and $X_a^{l,g}$ satisfy the relations

$$X_w^l + X_a^l = 1 \tag{2-5}$$

and

$$X_w^g + X_a^g = 1 \tag{2-6}$$

Diffusion of water in the aqueous phase is neglected. The liquid and gas pressures are related through the capillary pressure

$$P_l = P_g - P_c \tag{2-7}$$

P_c is typically defined as effective saturation.

Mass transfer in the gas phase may be enhanced by binary gas diffusion. The effective binary gas diffusion coefficient is defined using temperature, pressure, and material properties by

$$D_g^{\text{eff}} = \omega\,\tau\,\varphi\,s_g D_g^o \frac{P_o}{P_g}\left[\frac{T + T_o}{T_o}\right]^{\theta} \tag{2-8}$$

where D_g^o , T_o and P_o denote reference binary gas diffusion, temperature, and pressure. τ is tortuosity, θ is an empirical constant, and ω is an enhancement factor (Walton and Lichtner, 1995). The enhancement factor is usually considered inversely proportional to the gas saturation, s_g, which cancels from the expression for the effective gas diffusion coefficient.

Adding Eqs. (2-1) and (2-2) eliminates the diffusive terms providing the total mass balance equation for air and water as

$$\frac{\partial}{\partial t}\left[\varphi\left(s_l n_l + s_g n_g\right)\right] + \nabla \cdot \left(q_l n_l + q_g n_g\right) = Q_w + Q_a \tag{2-9}$$

Energy transfer is by convection and conduction. The energy balance equation, assuming thermodynamic equilibrium between rock and fluid, is given by

$$\begin{aligned}&\frac{\partial}{\partial t}\left[\varphi\left(s_l n_l U_l + s_g n_g U_g\right)\right] + \nabla \cdot \left(q_l n_l H_l + q_g n_g H_g\right)\\&+\frac{\partial}{\partial t}\left[\left(1-\mathrm{j}\right)\mathrm{C}_{\mathrm{P}}^{\mathrm{rock}}\mathrm{r}_{\mathrm{rock}}\mathrm{T}\right] - \nabla \cdot \kappa \nabla T = Q_e\end{aligned} \tag{2-10}$$

where $U_{l,g}$ denotes the total internal energy, $H_{l,g}$ the total enthalpy of the designated fluid phase, $\mathrm{C}_{\mathrm{P}}^{\mathrm{rock}}$ the heat capacity, κ the thermal conductivity, and Q_e a source term. Heat produced by chemical reaction is not included in the present version of the code. Energy transfer by radiation is only included at a boundary.

Vapor-pressure lowering of water-phase behavior resulting from capillary forces is defined by Kelvin's equation

$$P_v = P_{\mathrm{sat}}\left(T\right)e^{-P_c / n_l R T} \tag{2-11}$$

where P_v represents vapor pressure, P_{sat} the saturation pressure of pure water, T the absolute temperature, and R the gas constant. Note that the density of the liquid phase, n_l, is represented on a molar basis.

2.2 Model Parameters

Spatially variable values for porosity, absolute rock permeability (variable in three spatial directions), tortuosity, thermal conductivity, and media characteristic curves for relative permeability and capillary pressure can be specified. Capillary saturation relations provided in METRA are van Genuchten (1980), linear, and Brooks-Corey (Brooks and Corey, 1966) functions.

Liquid-phase relative permeability, k_{rl}, is calculated using the Mualem relationship (Mualem, 1976)

$$k_{rl} = \sqrt{s_l^{\mathrm{eff}}}\left\{1-\left[1-\left(s_l^{\mathrm{eff}}\right)^{1/m}\right]^m\right\}^2 \tag{2-12}$$

where capillary pressure, P_c, is related to saturation by the van Genuchten relationship (van Genuchten, 1980)

$$s_l^{\text{eff}} = \left[1 + \left(\alpha \left|P_c\right|\right)^n\right]^{-m} \tag{2-13}$$

where effective liquid saturation, s_l^{eff}, is defined by

$$s_l^{\text{eff}} = \frac{s_l - s_l^r}{s_l^o - s_l^r} \tag{2-14}$$

and where r and o denote residual and maximum saturations. The symbols α and m are the van Genuchten parameters. m is related to n in Eq. (2-13) by $m = 1 - 1/n$.

The gas-phase relative permeability, k_{rg}, is defined in terms of k_{rl}

$$k_{rg} = 1 - k_{rl} \tag{2-15}$$

The Brooks-Corey functions for liquid- and gas-phase relative permeabilities are defined by (Brooks and Corey, 1966)

$$k_{rl} = s_*^4 \tag{2-16}$$

and

$$k_{rg} = \left(1 - s_*^2\right)\left(1 - s_*\right)^2 \tag{2-17}$$

where saturation, s_*, is defined by

$$s_* = \frac{s_l - s_l^r}{1 - s_l^r - s_g^r} \tag{2-18}$$

Note that for the Brooks-Corey functions, $k_{rl} + k_{rg} \neq 1$, except for $s_* = 0$.

The linear relations for liquid- and gas-phase relative permeabilities are defined

$$k_{rl} = s_{\text{lin}} \tag{2-19}$$

and

$$k_{rg} = 1 - k_{rl} \tag{2-20}$$

where saturation, s_{lin}, is defined by

$$s_{\text{lin}} = \frac{s_l - s_l^r}{1 - s_l^r} \tag{2-21}$$

Thermal conductivity is also defined as a function of saturation (Somerton, et al., 1974)

$$\kappa = \kappa_{\text{dry}} + \sqrt{s_l^{\text{eff}}}\left\{\kappa_{\text{sat}} - \kappa_{\text{dry}}\right\} \tag{2-22}$$

where κ_{sat} and κ_{dry} are the thermal conductivities for fully saturated and dry conditions.

2.3 Formulation of Active Fracture Model

An active fracture model for unsaturated flow through fractured rocks proposed by Liu, et al. (1998) is based on a hypothesis that only a portion of connected fractures is active in conducting water. The hypothesis stipulates that (i) all connected fractures are active if the system is fully saturated, (ii) all fractures are inactive if the system is at residual saturation, and (iii) the fraction of fractures that are active is related to water flux through the fractures. Liu, et al. (1998) proposed that the fraction of active fractures be a power function of effective water saturation in connected fractures. The liquid-phase relative permeability function defined in Eq. (2-12) is modified to

$$k_{rl} = \left(s_l^{\text{eff}}\right)^{\frac{1+\gamma}{2}}\left\{1 - \left[1 - \left(s_l^{\text{eff}}\right)^{\frac{1+\gamma}{2}}\right]^m\right\}^2 \tag{2-23}$$

where the van Genuchten relationship between effective saturation and capillary pressure in Eq. (2-13) is modified to

$$s_l^{\text{eff}} = \left[1 + \left(\alpha\left|P_c\right|\right)^{\frac{n}{1-\gamma}}\right]^{-m} \tag{2-24}$$

where γ is a positive constant depending on the properties of the fracture network. The gas-phase relative permeability function is defined by the Brooks-Corey function in Eq (2-17). Values for k_{rg}, k_{rl}, and P_c for the active fracture model are linearly interpolated from specified values of saturation included as a look-up table in MULTIFLO code Version 1.5.1.

2.4 Formulation of Dual Continuum Model

The dual continuum model formulation as defined by MULTIFLO is conceptually equivalent to the dual permeability model formulation used in recent U.S. Department of Energy numerical simulations (TRW Environmental Safety Systems, Inc., 2000). The dual continuum model and dual permeability model conceptualization provides separate continua for the matrix and the

fractures. The dual continua are coupled throughout the model domain by transfer functions for heat and mass transfer between the fractures and matrix. Use of a dual continuum model increases the complexity of the numerical model used in the simulations, but offers the potential to realistically partition flow between matrix and fractures. The following is a description of key components to the dual continuum model incorporated in MULTIFLO and used in the numerical analyses of the Drift-Scale Heater Test.

One of the critical parameters in a dual continuum model-based formulation is the model block size. The fracture-matrix distances (in each dimension) are related, but not equivalent, to model block dimensions. The model block dimension, *d,* is the distance between the center of the matrix block and the center of the fracture defining the edge of the model block. For the case where the element is a cube, $d = l/2 + \delta/2$, where l is the length of the matrix block, and δ is the fracture aperture. Fracture aperture is calculated using model block size, matrix block size, and fracture porosity. Model block size directly affects two model properties: (i) the interfacial area between the matrix and fracture continua in a dual continuum model and (ii) the gradients that drive heat and mass between the two continua. In particular, increasing model block size reduces the area available for heat and mass transfer between the matrix and fracture continua and increases the distance over which changes in pressure and temperature occur, thereby reducing their respective gradients.

The interfacial area between the two continua, A_{fm}, is defined using matrix block dimensions, l_i, where $i = x, y,$ and z. For two dimensions, the interfacial area is defined by

$$A_{fm} = 2\left(1-\varphi_f\right)\left[\frac{1}{l_x}+\frac{1}{l_z}\right] \tag{2-25}$$

which, for a cubic block geometry in two dimensions (i.e., $l_x = l_z$), becomes

$$A_{fm} = 4\left(\frac{1-\varphi_f}{l}\right) \tag{2-26}$$

where φ_f is fracture porosity.

Mass flow across the matrix/fracture interface, $Q_{l-\text{mass}}$, is directionally dependent. When $P_{lm} > P_{lf}$, liquid flow from the matrix to the fracture continuum is defined by

$$Q_{l-\text{mass}} = \frac{A_{fm}A_{\text{mod}}}{\mu_l} k_{\text{harmonic},\,l} k_{rl,m} \frac{P_{lf}-P_{lm}}{d} \tag{2-27}$$

where the *m*, *f*, *l*, and *r* subscripts denote matrix, fracture, liquid, and relative.

A_{mod} is a modifier term included to allow a reduction, but not an increase, in the interfacial area between the matrix and fracture continua. The liquid-phase relative permeability function for

fracture to matrix flow, $k_{rl,f\to m}$, need not be the same, thereby providing additional flexibility to the model.

The harmonic mean for liquid permeability is expressed as

$$k_{\text{harmonic},l} = \frac{k_f\, k_m}{k_f + k_m} \tag{2-28}$$

The liquid-phase relative permeability function for fracture-to-matrix flow, $k_{rl,f\to m}$, need not be the same as for the fracture continuum, $k_{rl,f}$. This additional flexibility introduced in MULTIFLO Version 1.5.1 permits additional reduction in flow consistent with the active fracture model. This additional reduction only applies to liquid flow from fractures to matrix. Heat and gas flow and flow from matrix-to-fracture are not affected. Within the active fracture model, $k_{rl,f\to m}$ is approximated as

$$k_{rl,f\to m} \cong \left(S_l^{\text{eff}}\right)^{1+\gamma} k_{rl,f} \tag{2-29}$$

For $P_{lf} > P_{lm}$ liquid flow from the fracture to the matrix is defined by

$$Q_{l-\text{mass}} = \frac{A_{fm} A_{\text{mod}}}{\mu_l} k_{\text{harmonic},l} k_{rl,f\to m} \frac{P_{lf} - P_{lm}}{d} \tag{2-30}$$

An analogous form of Eq. (2-27) defines mass flow of gas between the matrix and fracture continua.

$$Q_{g-\text{mass}} = \frac{A_{fm} A_{\text{mod}}}{\mu_g} k_{\text{harmonic},g} k_{rg} \frac{P_{gf} - P_{gm}}{d} \tag{2-31}$$

Note that mass flow of gas between the matrix and fracture continua is not directional, that is, the A_{mod} for matrix to fracture gas flow is equal to the A_{mod} for fracture to matrix gas flow.

Analogous to mass flow are expressions and relationships for heat flow. Heat flow across the matrix fracture interface is defined as

$$Q_{\text{heat}} = A_{fm} A_{\text{mod}}\, \kappa_{\text{arithmetic}} \frac{T_f - T_m}{d} \tag{2-32}$$

Note that heat transfer and mass transfer across the matrix/fracture interface are coupled processes, but each responds to its respective driving forces calculated for the same distance, d. Gradients that drive mass and heat transfer are decreased when the block dimensions are

increased (i.e., the differences in pressure or temperature between the two continua remain the same for each model element while the distance over which the difference occurs increases with an increased block size, thereby reducing the gradients).

Either time-dependent Neumann (constant flux), Dirichlet (constant field variables), or mixed boundary conditions may be specified in MULTIFLO. Time-varying heat and mass sources and sinks may be designated at specified nodal locations. Time-varying boundary conditions, sources, or sinks are specified in tabular form and are linearly interpolated corresponding to the midpoint of the timestep.

3 NUMERICAL SOLUTION

METRA is based on a fully implicit formulation using a variable substitution approach. Space discretization is based on a block-centered grid using an integral finite-volume difference scheme. This approach is suitable for a structured and unstructured grid with arbitrary interblock grid connectivity and any polygon block boundary. Flow through fractured media may be represented by the dual continuum model or using an equivalent continuum medium where the dual continuum is represented by an equivalent single continuum (Pruess and Narasimhan, 1985; Klavetter and Peters, 1986).

Three primary variables are required to describe a two-phase nonisothermal system consisting of two species, water and air. The chosen primary variables are listed in Table 3-1, where P_l is the liquid pressure for a pure liquid system and P_g the total gas pressure for a two-phase or pure gas-phase system. X_a denotes the mole fraction of air with partial pressure P_a, s_g denotes gas saturation, and T denotes temperature. Note that gas saturation is related to liquid saturation by $s_g + s_l = 1$.

Three primary equations are solved by METRA: (i) total mass balance, (ii) air mass balance, and (iii) energy balance. The three equations are simultaneously solved for each grid block by the tridiagonal Thomas algorithm for one-dimensional systems and by the WATSOLV package (van der Kwaak, et al., 1995) for both two-dimensional and three-dimensional systems. The WATSOLV package is based on incomplete factorization accelerated by employing generalized minimum residual or biconjugate gradient stabilized procedures (van der Kwaak, et al., 1995).

Table 3-1. Choice of Primary Variable for Different Fluid States

Fluid State	Primary Variables
Single-phase liquid	P_l, X_a, T
Two phase	P_g, P_a, s_g
Single-phase gas	P_g, P_a, T

4 DRIFT-SCALE HEATER TEST MODEL

The Exploratory Studies Facility Thermal Test Facility (Alcove 5) is located in the Topopah Spring middle nonlithophysal unit, within the horizon of a potential Yucca Mountain repository (TRW Environmental Safety Systems, Inc., 1997a). The Topopah Spring middle nonlithophysal unit is approximately 30–40 m [98–131 ft] thick at the location of the Drift-Scale Heater Test, overlain by the Topopah Spring upper lithophysal and underlain by the Topopah Spring lower lithophysal units. Alcove 5 is at Construction Station 28 + 27 (a coordinate system in meters following the axis of the Exploratory Studies Facility and originating at the North Portal), just past the bend from the North Ramp to the Main Drift (as shown in Figure 4-1, from TRW Environmental Safety Systems, Inc., 1997a). The Drift-Scale Heater Test test block was characterized prior to the onset of heating. Onsite characterization of the local geology, *in-situ* hydrology, and local rock-mass quality were supplemented with laboratory tests of thermal-hydrological-mechanical-chemical properties. Characterization data collected from the single-heater test block (Tsang, et al., 1999; Blair, et al., 1998; Tsang and Birkholzer, 1999) provided additional information on the Drift-Scale Heater Test horizon. The ensemble of these data provides the characterization of the Drift-Scale Heater Test block and model parameters and is consistent with results from previous nonthermal test studies by Brechtel, et al. (1995), Birkholzer and Tsang (1997, 2000), and TRW Environmental Safety Systems, Inc. (1997a). The data are also consistent with parameter values cited in Civilian Radioactive Waste Management System Management and Operating Contractor (CRWMS M&O ,1998, 2001). Specific parameter values used in this analysis are from CRWMS M&O (2001).

The primary components of Alcove 5, indicated in Figure 4-2 [also taken from TRW Environmental Safety Systems, Inc. (1997a)], are the site of the single-heater test (known as the thermomechanical alcove), the observation drift, the connecting drift, and the heated drift. A plan-view schematic of the relative placement of the heated drift to the observation drift is shown in Figure 4-1. The 5 m [16.4 ft] diameter, 47.5 m [155.8 ft] long heated drift is closed at the east end by a thermal bulkhead. Approximately 12.5 m [41.0 ft] of the west end of the heated drift is lined with cast-in-place concrete ground support. The heated drift diameter was expanded to 5.6 m [18.4 ft] along this section to allow for the concrete ground support. Concrete inverts with a thickness of 1.2 m [3.9 ft] at the drift midplane were placed along the entire floor of the heated drift to provide a flat surface. Thermal sources for the heated drift consist of 9 canister heaters, placed end to end on the floor of the heated drift, and 50 wing heaters (25 on either side), emplaced in horizontal boreholes drilled into the sidewalls of the heated drift approximately 0.25 m [0.8 ft] below the springline. The wing heaters are spaced 1.83 m [6.0 ft] apart. Each wing heater has 2 segments, both 5 m [16.4 ft] long, with a larger power output from the outer segment. The inner wing heater segment is separated from the heated drift by a space of 1.5 m [4.9 ft].

4.1 Drift-Scale Heater Test Model Domain

The Drift-Scale Heater Test was numerically simulated with a three-dimensional model. The three-dimensional model was assembled with a series of 14 vertically oriented two-dimensional cross sections: 7 intersect the drift, and 7 are located beyond the terminus of the drift.
Two planes of vertical symmetry were assumed: 1 aligning with the axis of the heated drift, and 1 intersecting the axis of the heated drift mid-distance between thebulkhead and the terminus of the heated drift. Therefore, essentially one-fourth of the Drift-Scale Heater Test was included

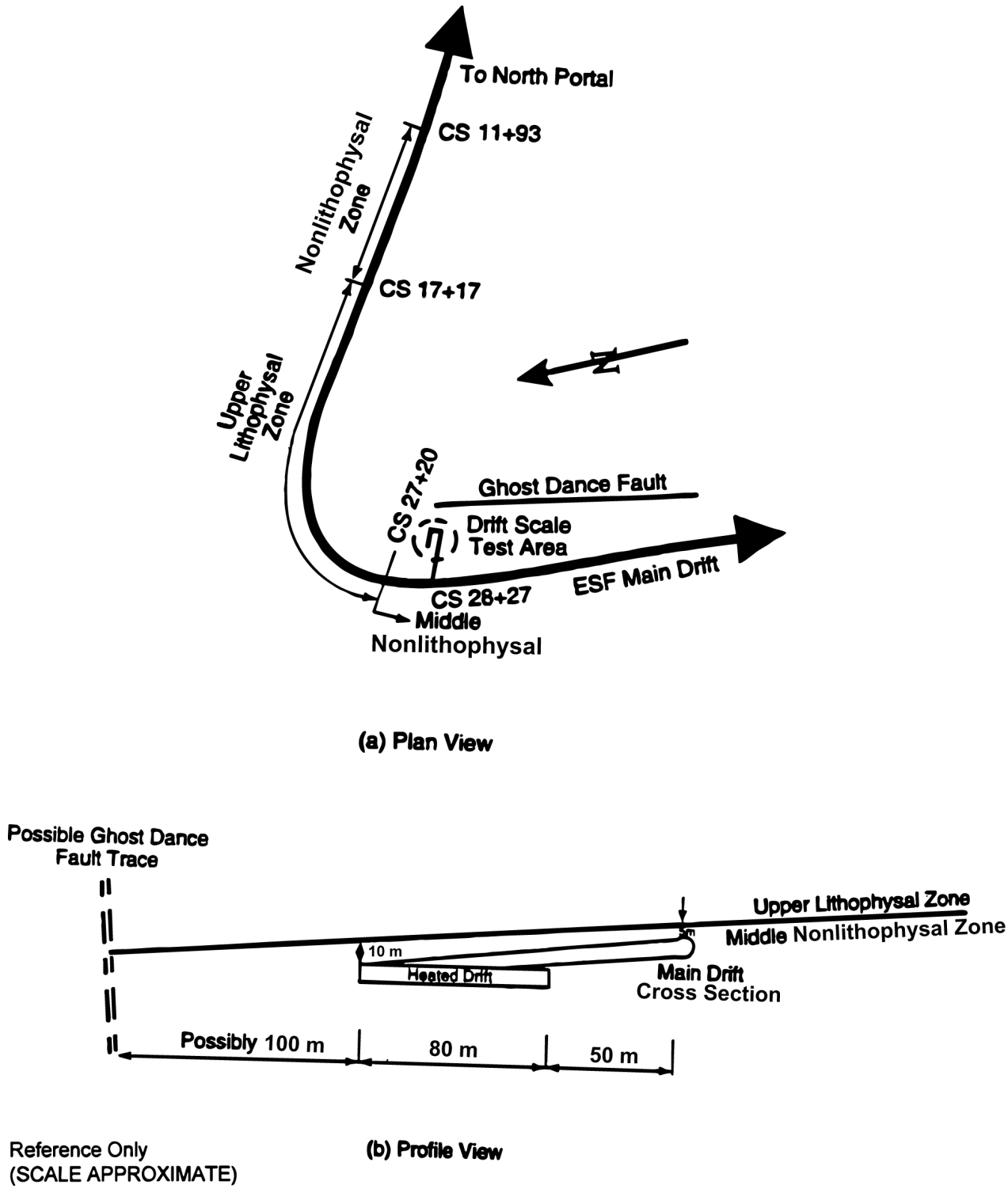

Figure 4-1. (a) Plan View at the North Ramp of the Exploratory Studies Facility and Drift-Scale Test Area, (b) Cross Section of the Drift-Scale Test Area Showing the Heated Drift in Relation to the Main Drift and Contact Between Geological Units (TRW Environmental Safety Systems, Inc., 1997a) (Note: 1 m = 3.2808 ft)

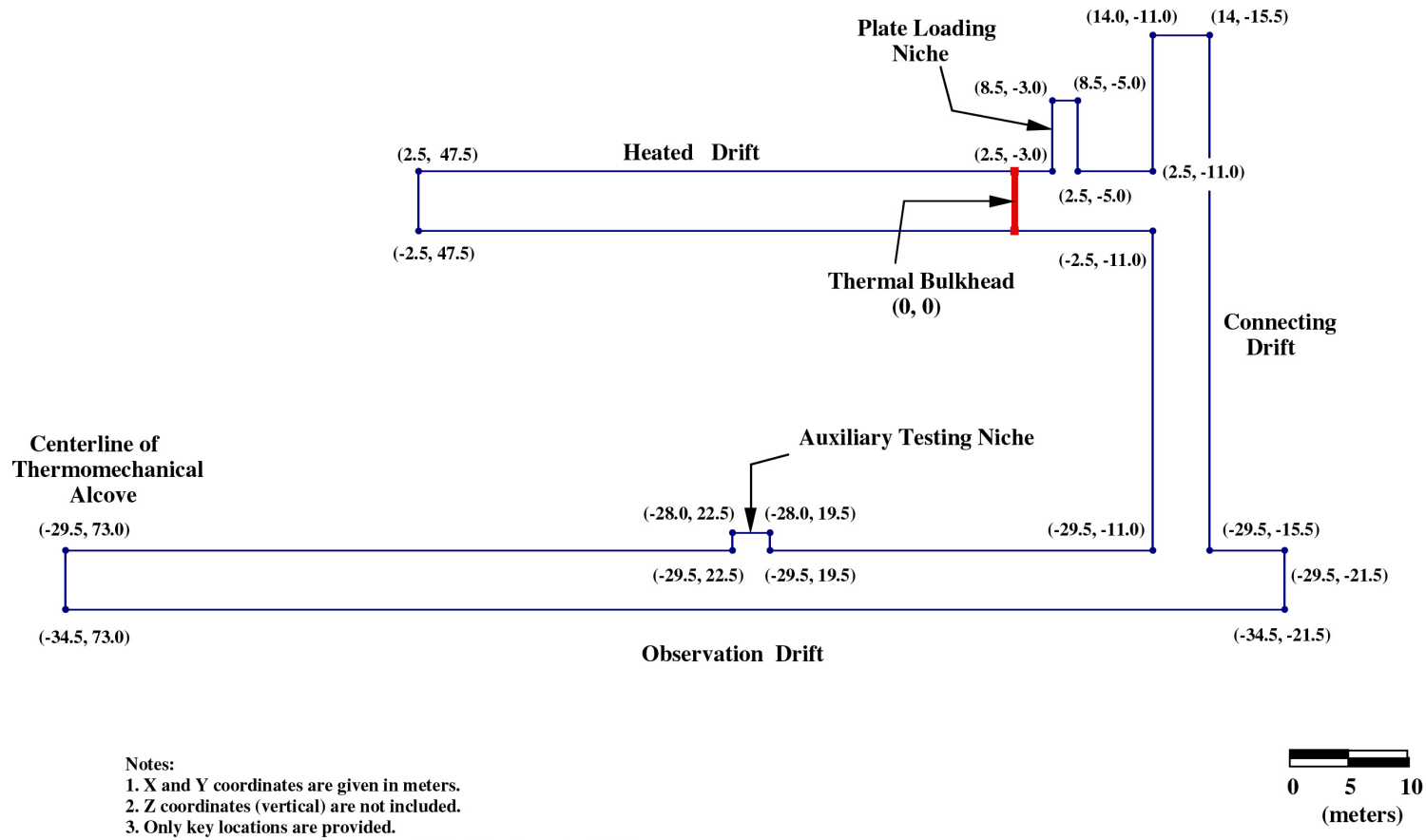

Notes:
1. X and Y coordinates are given in meters.
2. Z coordinates (vertical) are not included.
3. Only key locations are provided.
4. Coordinates are based on design with the following as-builts tolerances:
   Horizontal alignment = - 0 to + 0.5m
   All other = - 0 to + 0.3m

Figure 4-2. Plan-View Schematic of the Primary Components of Alcove 5 and the Drift-Scale Heater Test Region (TRW Environmental Safety Systems, Inc., 1997b) (Note: 1 m = 3.2808 ft)

in the numerical model. The modeled area extends 200 m [656 ft] vertically with the center of the heated drift placed at the center of the numerical model and 100 m [328 ft] horizontally from the drift center. The boundaries for this model were extended from distances reasonably needed for thermohydrological simulations to for allow temperature predictions needed at greater distances required by thermal-mechanical simulations.

The two-dimensional slice of the grid with 1,123 nodes in the planes intersecting the drift is illustrated in Figure 4-3. A closeup of the two-dimensional slice of the the grid in the vicinity of the heated drift is shown in Figure 4-4, which illustrates the finer mesh resolution in areas expected to experience large temperature, saturation, and pressure gradients. Planes beyond the terminus of the drift had an additional 52 nodes to fill in the drift cavity for a total of 1,175 nodes (not shown). The full three-dimensional model, therefore, has 16,068 nodes in each continuum for a total of 32,136 nodes. The model domain is modeled as three hydrostratigraphic units, the Topopah Spring upper lithophysal (tsw33), Topopah Spring middle nonlithophysal (tsw34), and Topopah Spring lower lithophysal (tsw35) of the Topopah Spring welded unit.

4.2 Model Property Assignment

Basecase property values for tsw33, tsw34, and tsw35 were taken from CRWMS M&O (2001). These values are summarized in Tables 4-1 through 4-3. Fracture permeability is expressed in terms of intrinsic values. Bulk fracture permeability can be calculated by dividing the intrinsic values by the fracture porosity. A block size of 0.40 m [1.3 ft] was uniformly assigned to the entire model domain for the basecase. The wing heaters had the same hydraulic properties as the adjoining rock (tsw34) in the basecase but had modified hydraulic properties in two simulations to simulate the effect of the wing heater borehole.

4.3 Boundary and Initial Conditions

The vertical boundaries of the model were specified as adiabatic with no fluid flow. The top boundary for the basecase was prescribed as a specified flux. The bottom boundary was prescribed as a drainage boundary with specified pressure, temperature, and saturation. The mixed boundary condition at the top allows gas and heat transport in or out of the model while maintaining pressure and temperature as specified. Water flux at the top boundary was introduced into the fracture continuum. The heated drift was not explicitly included in the model; instead, the heated drift wall was modeled as a Dirichlet boundary (constant pressure), and heat from the floor canisters was applied directly to the heated drift walls. The effect of the pressure Dirichlet boundary at the heater drift wall allows the removal of sensible heat transported by water vapor. Heat removal from the drift wall by either conduction or radiation is not explicitly included in the simulation. Heat loss through the drift wall by these two mechanisms was implicitly incorporated by reducing the heat load imposed at the drift wall by variable amounts (i.e., 20 percent) to evaluate this source of heat loss.

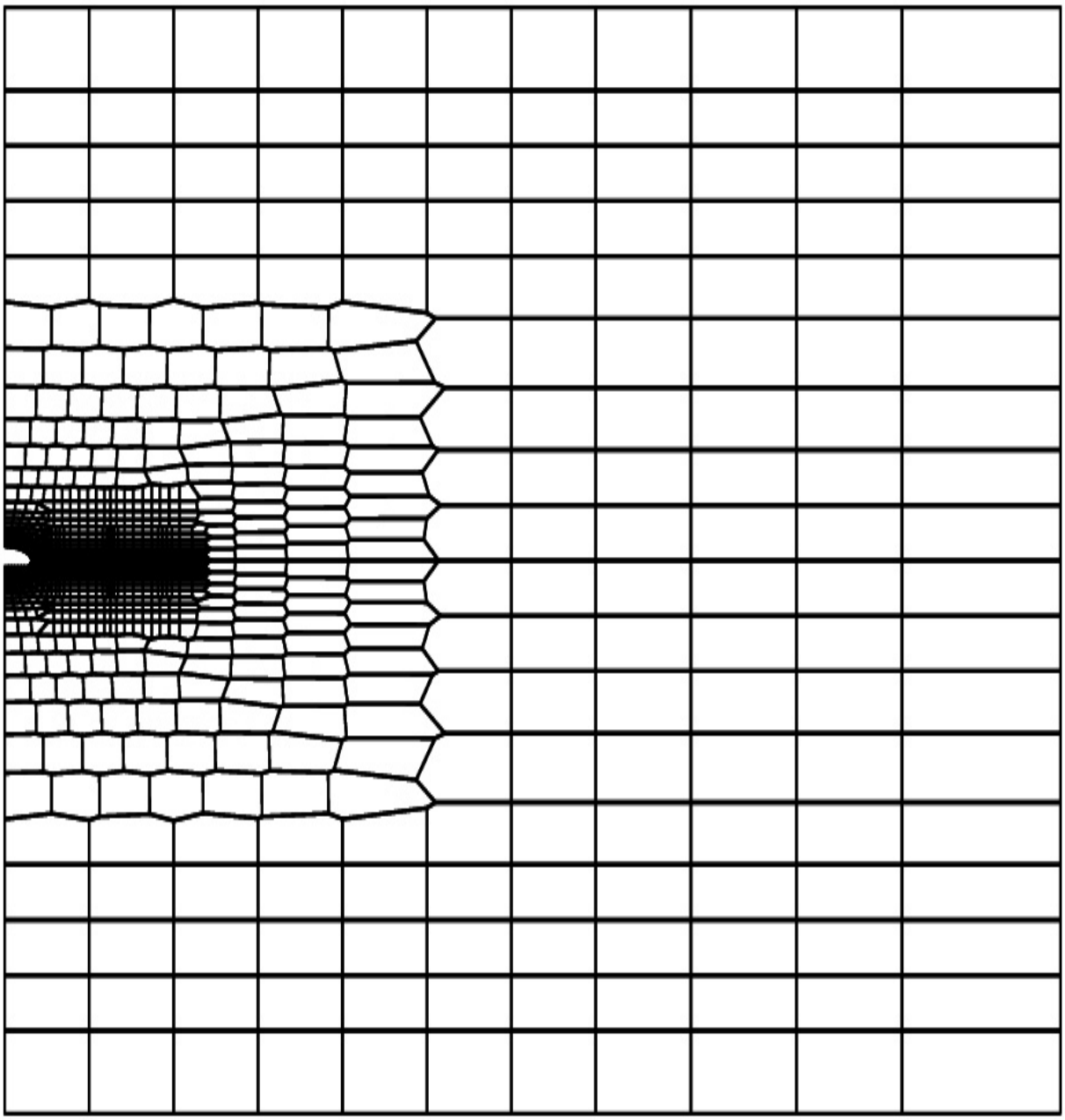

Figure 4-3. Vertically Oriented Grid Discretization of the Drift-Scale Heater Test. The Illustrated Section Is for the Modeled Block with the Drift.

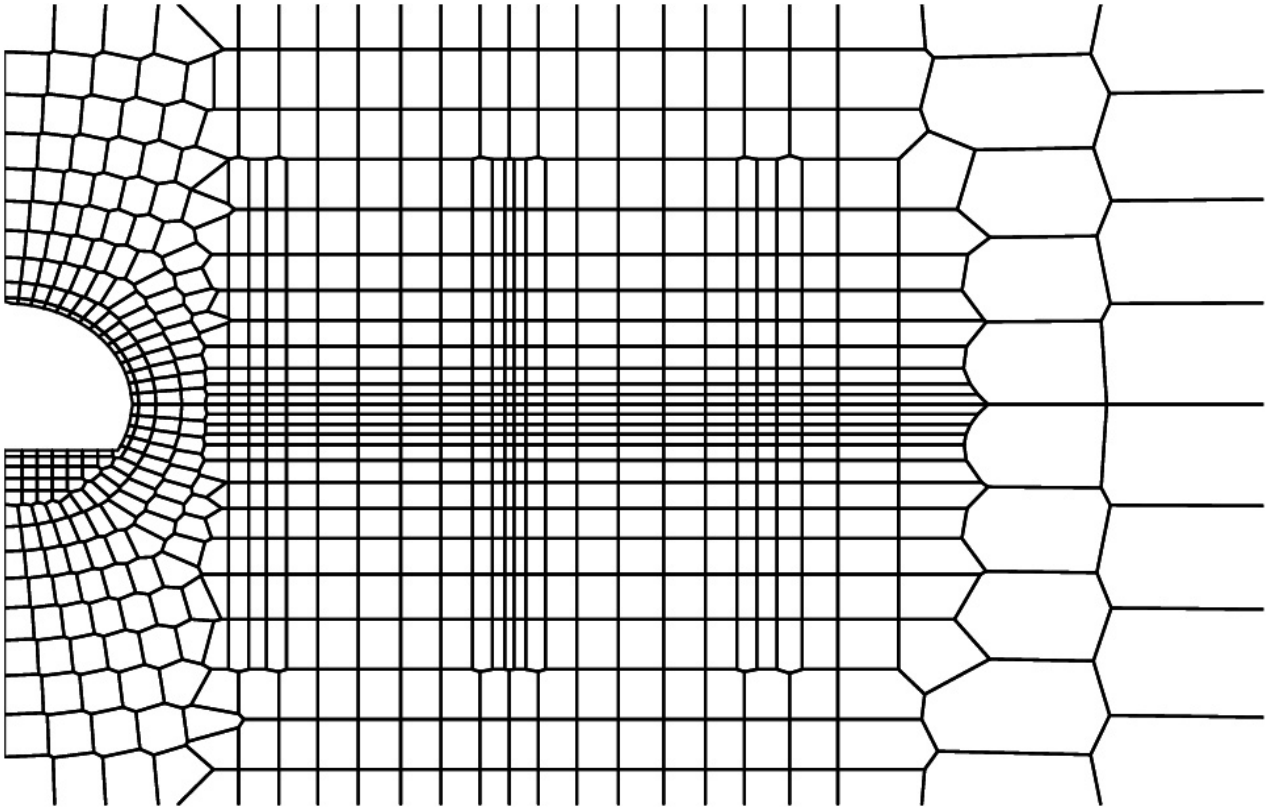

Figure 4-4. Closeup of the Grid Discretization Proximal to the Heated Drift and Wing Heaters. The Illustrated Section Is for the Modeled Block with the Drift.

Table 4-1. Matrix Hydraulic Properties Taken from Total System Performance Assessment–Viability Assessment Thermal-Hydrological Parameter Set*					
Unit	**Porosity**	**Permeability (m^2) [ft^2]**	**s_r**	**α (Pa^{-1})**	**m**
tsw33 (Tptpul)†	0.154	3.08×10^{-17} [3.31×10^{-16}]	0.12	2.13×10^{-5}	0.298
tsw34 (Tptpmn)‡	0.110	4.07×10^{-18} [4.38×10^{-17}]	0.19	3.86×10^{-6}	0.291
tsw35 (Tptpll)§	0.131	3.04×10^{-17} [3.31×10^{-16}]	0.12	6.44×10^{-6}	0.236

*CRWMS M&O. "Multiscale Thermohydrologic Model." ANL–EBS–MD–000049. Rev. 00 ICN02. North Las Vegas, Nevada: CRWMS M&O. 2001
† Topopah Spring upper lithophysal
‡ Topopah Spring middle nonlithophysal
§ Topopah Spring lower lithophysal

Table 4-2. Fracture Hydraulic Properties*						
Unit	**Porosity**	**Permeability Vertical (m^2)[ft^2]**	**Permeability Horizontal (m^2)[ft^2]**	**s_r**	**α (Pa^{-1})**	**m**
tsw33 (Tptpul)†	0.0066	5.50×10^{-13} [5.92×10^{-12}]	5.50×10^{-13} [5.92×10^{-12}]	0.01	1.46×10^{-3}	0.608
tsw34 (Tptpmn)‡	0.010	2.76×10^{-13} [2.97×10^{-12}]	2.76×10^{-13} [2.97×10^{-12}]	0.01	5.16×10^{-4}	0.608
tsw35 (Tptpll)§	0.011	1.29×10^{-12} [1.39×10^{-11}]	1.29×10^{-12} [1.39×10^{-11}]	0.01	7.39×10^{-3}	0.611

*CRWMS M&O. "Multiscale Thermohydrologic Model." ANL–EBS–MD–000049. Rev. 00 ICN02. North Las Vegas, Nevada: CRWMS M&O. 2001
† Topopah Spring upper lithophysal
‡ Topopah Spring middle nonlithophysal
§ Topopah Spring lower lithophysal

Table 4-3. Thermal and Physical Properties*					
Unit	**Thermal Conductivity–Dry (W/m-K)**	**Thermal Conductivity–Wet (W/m-K)**	**Rock-Specific Heat (J/kg-K)**	**Rock Density (kg/m^3)**	**F_{ma} (m^2/m^3)[ft^2/ft^3]**
tsw33 (Tptpul)†	0.79	1.68	882	2510	5×10^{-4} [1.54×10^{-4}]
tsw34 (Tptpmn)‡	1.56	2.33	948	2530	1.23×10^{-3} [3.75×10^{-4}]
tsw35 (Tptpll)§	1.20	2.02	900	2540	5×10^{-4} [1.54×10^{-4}]

*CRWMS M&O. "Multiscale Thermohydrologic Model." ANL–EBS–MD–000049. Rev. 00 ICN02. North Las Vegas, Nevada: CRWMS M&O. 2001
† Topopah Spring upper lithophysal
‡ Topopah Spring middle nonlithophysal
§Topopah Spring lower lithophysal

The temperature was specified as 22 °C [71.6 °F] and 24 °C [75.2 °F] at the top and bottom boundaries for a geothermal gradient of 0.01 °C/m [0.005 °F/ft]. A static gas pressure difference of 1,920 Pa between the top and bottom boundaries was specified to impose a gas gradient consistent with ambient conditions. This pressure is equivalent to a 200-m [656-ft] tall column of air at standard pressure and temperature. Gas pressures of 88,920 Pa at the bottom and 87,000 Pa at the top establish a gas pressure at the Drift-Scale Heater Test horizon of slightly less than 88,000 Pa, consistent with observed gas pressures and gas pressure gradients (Bodvarsson and Bandurraga, 1997).

Sensitivity analyses conducted in a previous study evaluated how different property assignments and boundary and initial conditions affect the ambient matrix saturation before the Drift-Scale Heater Test (Green, et al., 2000, 2001). Ambient saturation was determined by simulating flow in the absence of heat at the Drift-Scale Heater Test for sufficiently long periods of time that steady-state flow conditions were approximated. The steady-state simulations were run without the presence of the drift to avoid the shadow effects of the drift opening on ambient saturation. Steady-state flow conditions were usually approximated in about 10^7 years.

Ambient matrix saturation was selected as the key state variable to evaluate the appropriateness of the pretest (i.e., steady-state or ambient) conditions for the conceptual and numerical models used to simulate the Drift-Scale Heater Test. This selection was made because of the sensitivity of saturation to changes in model design and the ability to directly measure matrix saturation on core and grab samples collected at the site. A matrix saturation of 0.92 in the tsw34 (Topopah Spring middle nonlithophysal) was designated the target saturation. This target saturation is close to the value of 0.924 measured on samples collected at the Drift-Scale Heater Test (TRW Environmental Safety Systems, Inc., 2000).

Simulations run to determine the steady-state conditions encountered a potential conflict when the most current property values were used in the simulation. In particular, simulations that included a block size of 0.40 m [1.3 ft], infiltration rate of 3.0 mm/yr [0.0098 ft/yr], and the media property values documented in CRWMS M&O (2001) predicted steady-state saturations greater

than 0.99, much greater than the documented ambient matrix saturations (i.e., 0.92). Sensitivity analysis results indicated that lower saturations can be achieved by either significantly decreasing infiltration {from 3.0 mm/yr [0.0098 ft/yr] to approximately 0.07 mm/yr [0.0002 ft/yr]} or increasing the block size {from 0.4 m [1.3 ft] to approximately 5.0 m [16.4 ft]}. Although fracture mapping indicates a block size of 0.4 m [1.3 ft], not all fractures are necessarily hydraulically active. It is not clear how to accurately incorporate into models the difference between mapped fractures and hydraulically active fractures. Increasing block size and incorporating an active fracture conceputualization into the model are two possible approaches. The ramifications of increased block size are not fully understood and are being evaluated.

4.4 Previous Drift-Scale Heater Test Modeling Results

Analyses reported in this document have built on previous studies performed at the Center for Nuclear Waste Regulatory Analyses. Summaries of these studies are included here.

Model parameters evaluated in a previous study (Green, et al., 2000) were infiltration rate, block size, liquid flow from matrix to fracture interaction area, the upper boundary condition, and fracture permeability. These parameters were selected for investigation because sensitivity analysis results indicated that changes in these property values have a significant effect on predicted matrix saturation. Specific changes to model parameters evaluated were

- Surface boundary changed from Neumann to mixed with specified flux and constant temperature and pressure
- Block size varied from 0.25 m [0.82 ft] to 20 m [65.6 ft]; infiltration flux at the surface varied from 0.00036 mm/yr [0.0000012 ft/yr] to 3.6 mm/yr [0.012 ft/yr]
- Anisotropic fracture permeability decreased by three orders of magnitude in the x-, y-, and z-directions from the basecase values

As demonstrated in the investigation by Green, et al. (2000), changes in values assigned to fracture permeability had negligible effects on ambient matrix saturation but did affect temperatures and saturations predicted for the heating phase of the Drift-Scale Heater Test. Changes in block size and infiltration rate proved to have a significant effect on ambient matrix saturation, as illustrated in Figure 4-5 (a through d). An increase in block size decreased the ambient steady-state saturation. This effect was more pronounced for a smaller value of A^*_{mod} (fracture-matrix area modification factor) [i.e., 1.23×10^{-4} in Figure 4-5 (a and b)] than for a larger value of A^*_{mod} [i.e., 1.0 in Figure 4-5 (c and d)] for both high {i.e., 3.6 mm/yr [0.012 ft/yr]} and low {i.e., 0.072 mm/yr [0.0002 ft/yr]} infiltrations. (The A^*_{mod} nomenclature is not used in MULTIFLO code Version 1.5.1.) In fact, it is possible to have a reasonable ambient steady-state saturation of 0.92 with an infiltration rate of 3.6 mm/yr [0.012 ft/yr] if block size is increased to approximately 6 m [19.7 ft] to 7 m [23 ft] [Figure 4-5 (a)].

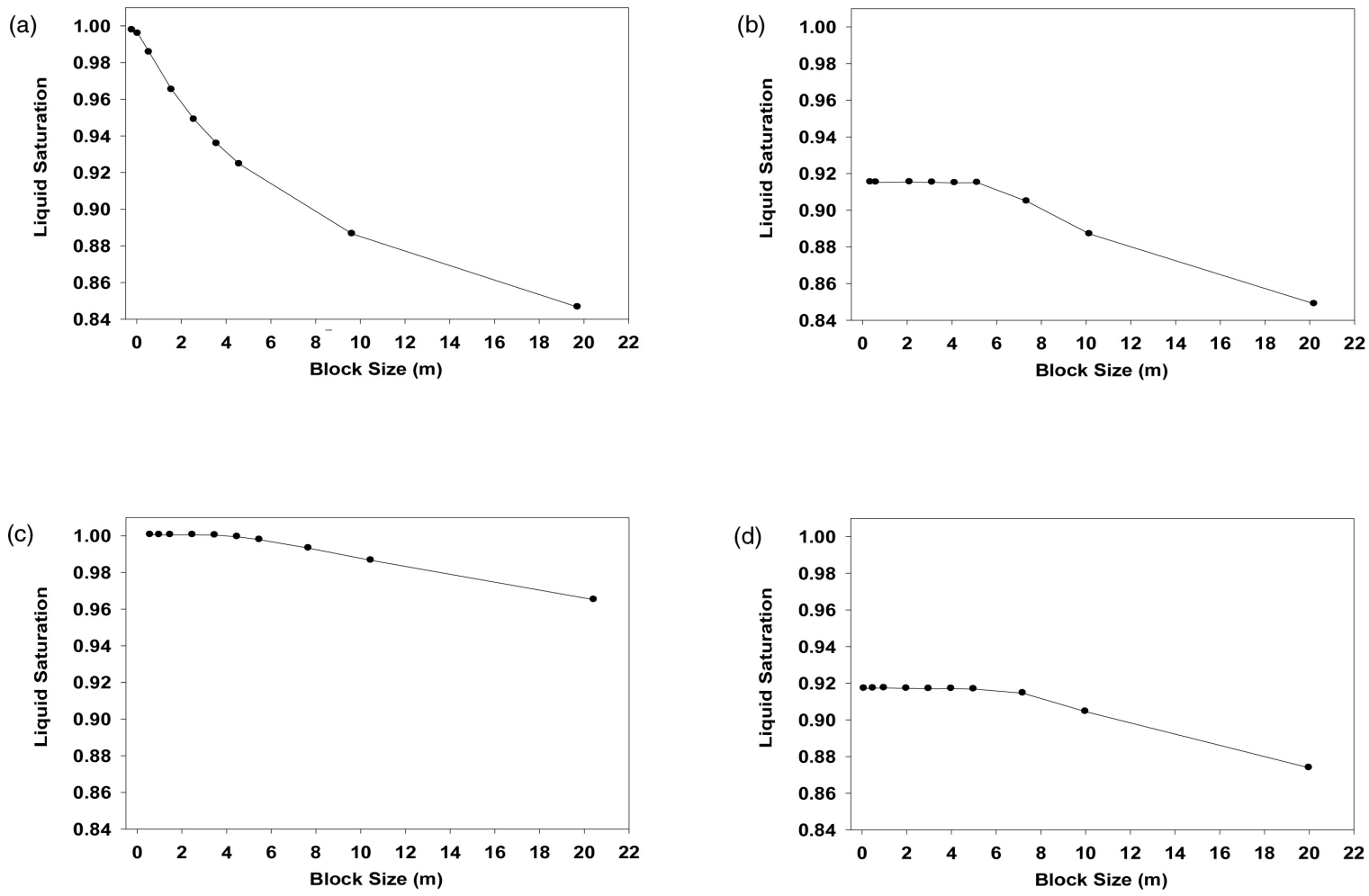

Figure 4-5. Ambient Matrix Saturation Predicted for the Topopah Spring Middle Nonlithophysal at a Point 8.9 m Above the Center of the Heated Drift Versus Model Block Size for a Value of 1.23×10^{-3} Assigned to A^*_{mod} in the Topopah Spring Middle Nonlithophysal with Infiltration Rates of (a) 3.6 mm/yr and (b) 0.072 mm/yr and for a Value of 1.0 Assigned to A^*_{mod} in the Topopah Spring Middle Nonlithophysal with Infiltration Rates of (c) 3.6 mm/yr and (d) 0.072 mm/yr (Note: 1 m = 3.2808 ft; 1 mm = 0.003281 ft)

Additional numerical simulations were performed (Green, et al., 2001) to evaluate the effects of changes to fracture permeability, thermal conductivity, the active fracture model, and the matrix/fracture area modification factor had on predicted temperatures and saturations. The analyses evaluated the following effects:

- Intrinsic fracture permeability was reduced by factors of 10, 100, and 1,000.
- Thermal conductivity was increased and decreased by 20 percent.
- Steady-state and heated simulations were performed to evaluate the effects of the active fracture model (Liu, et al., 1998).
- The matrix/fracture area modification factor, A^*_{mod}, was varied from 1.0 to 1.0×10^{-4}.

The analyses by Green, et al. (2001) indicated reductions in the intrinsic fracture permeability had a significant effect on the evolution of temperature and formation of heat pipes. In particular, a thousand-fold reduction in intrinsic fracture permeability effectively removed most evidence of a heat pipe in the numerical predictions. A reduction in thermal conductivity had a slightly less significant effect on the evolution of temperature. Changes in A^*_{mod} and inclusion of the active fracture model had an effect on the preheating ambient saturation but no effect on temperature or saturation in the thermohydrological simulations. MULTIFLO code Version 1.5.1 no longer uses the matrix/fracture area modifier A^*_{mod}. The active fracture model incorporated in these earlier analyses assigned the same reduction in permeability to fracture to matrix flux and fracture flow.

4.5 New Simulations

4.5.1 Model Heat Source

Similar to previous Drift-Scale Heater Test simulations (Green, et al., 2000, 2001), heat was introduced into the current numerical model at the drift wall and at the inner and outer wing heaters. The drift cavity was not explicitly included in the model to avoid difficulties associated with representing the air space within the drift, radiative and convective heat transfer between the heater canisters and the drift wall, and the physics of heat and mass transfer at the drift-cavity/drift-wall boundary. The disadvantage to this simplification is that coupled thermohydrological processes at the drift wall cannot be directly or easily investigated. The heat-source levels were applied uniformly according to surface area to each of the 20 drift boundary elements at the 5 m [16.4 ft] diameter drift wall and to the 7 elements at the top of the invert. The 50 cylindrical wing heaters were not individually represented in the numerical model, but both the inner and outer wing heaters were represented as individual rectangular slabs, thereby smearing the heat deposition in the y-direction of the model. The 4.49 m [14.7 ft] long inner wing heater was set 1.67 m [5.48 ft] from the drift wall. The 4.59 m [14.7 ft] long outer heater was separated from the inner heater by 0.66 m [2.16 ft]. Both wing heaters were assigned a vertical thickness of 0.25 m [0.82 ft]. These dimensions are consistent with those provided in the as-built report (TRW Environmental Safety Systems, Inc., 1998a), with the exception of the wing heater thickness. The wing heaters were modeled as 0.25 m [0.82 ft] thick, rather than the reported diameter of 24 mm [0.079 ft], because of constraints on mesh resolution.

The increased thickness of the wing heaters will distort the resulting thermohydrological regime in the region close to the heat source; however, the effect should be negligible beyond a few tens of centimeters.

The design thermal load for the Drift-Scale Heater Test was 68.0 kW for the canister heaters and 143.0 kW for the cumulative wing heaters (85.8 kW at the outer wing heater and 57.2 kW for the inner wing heaters) for a total of 211 kW (TRW Environmental Safety Systems, Inc., 1998b). The Drift-Scale Heater Test has experienced decreased heat loads from the levels of the design heat loads since energizing the canisters and wing heaters in December 1997 (Figures 4-6 and 4-7). At the time of energizing, the canister heat load was approximately 52.8 kW, and the cumulative wing heater heat load was approximately 137 kW (TRW Environmental Safety Systems, Inc., 1998c). These power levels decreased immediately after heating started. The canister heat load increase from days 244 to 270 is correlated with a modification in the access drift and heated drift (outside the thermal bulkhead) ventilation system. A possible explanation is that the heat load was increased at the same time the ventilation was modified to maintain a constant temperature ramp up in the heated drift. The wing heaters also experienced an increase in heat load soon after day 244; however, this increase followed a rather precipitous decrease in the heater load from approximately 133 kW at day 185 to less than 130 kW by day 244 (TRW Environmental Safety Systems, Inc., 1998a). The cause of this precipitous heat load decrease is attributed to the loss of power to wing heater 29. Measured heater load values continued to decrease to approximately 52.3 kW for the canisters and to slightly more than 130 kW for the wing heaters by day 480 (TRW Environmental Safety Systems, Inc., 1999a) and to approximately 51.5 kW for the canisters and 128.2 kW for the wing heaters by day 700 (TRW Environmental Safety Systems, Inc., 1999b). After 800 days of heating, both the canister and wing heaters were incrementally decreased on 5 occasions to ensure measured drift wall temperatures did not exceed 200 °C [392 °F].

Model heat loads were designed to resemble the major features of the measured heat loads [DTN MO9807DSTSET01.000(113644), MO9810DSTSET02.000(113662), MO9906DSTSET03.000(113673), MO0001SEPDSTPC000(153836), MO0007SEPDSTPC.001(153707), MO0012SEPDSTPC.002(153708), MO0107SEPDSTPC.003(158321), MO0202SEPDSTTV.001(158320)]. The model thermal loads were ramped up to their starting power levels during a period of approximately 4.2 hours to avoid stability problems. The measured cumulative heat load for the canister heaters was approximated to remain constant at 52.0 kW until day 800 of heating. The canister heat was then linearly ramped down to 44 kW by day 1,000 and held at that heat load until day 1,200 at which time the heat load was linearly ramped down to 38 kW by day 1,500. In similar fashion, the heat load for the wing heaters was linearly ramped down from a starting cumulative heat load of 136.5 kW on day 1 to 129 kW by day 800. This heat load was then linearly ramped down to 108 kW by day 1,000 and held constant at 108 kW until day 1,200 at which time the heat load was linearly ramped down to 91 kW by day 1,500. At all times, 40 percent of the cumulative wing heater heat load was assigned to the inner heater, and 60 percent was assigned to the outer wing heater.

4.5.2 Model Features

Heat and mass transfer were simulated for the 4 years of the heating phase of the Drift-Scale Heater Test and compared to the Drift-Scale Heater Test data for the same period.

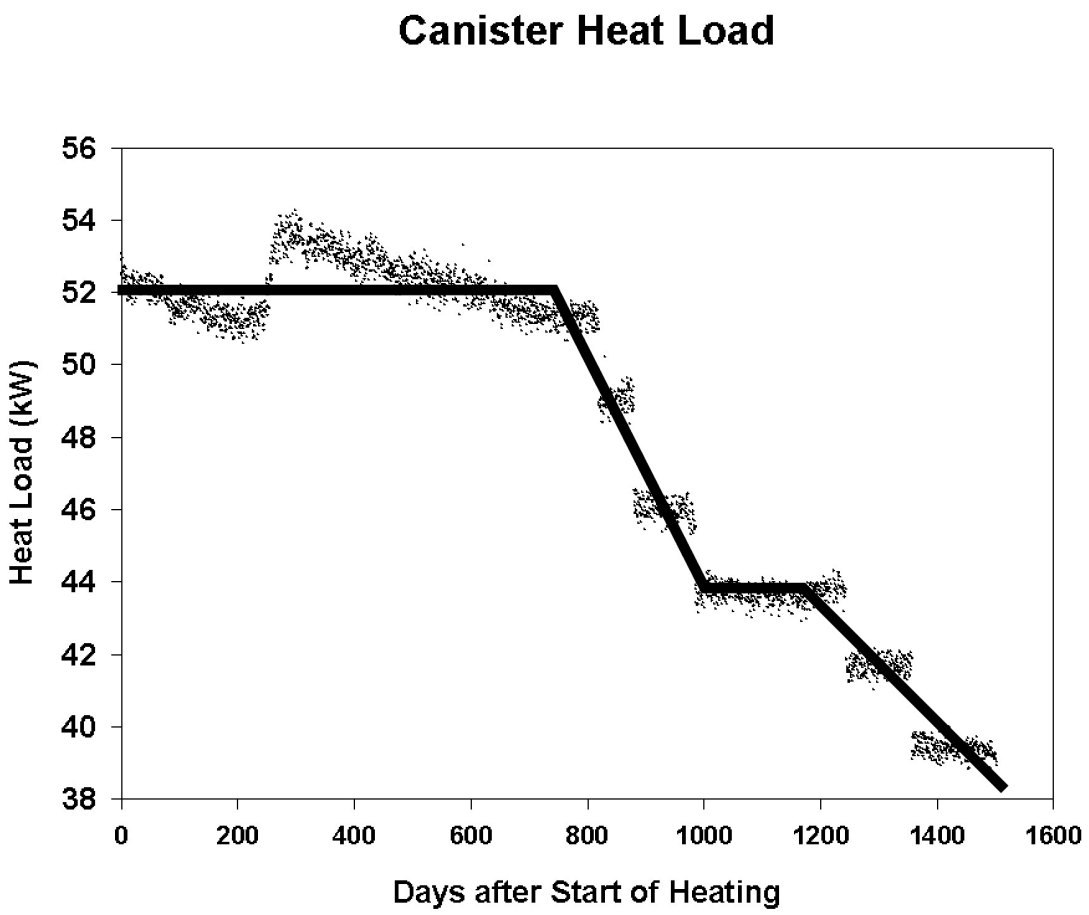

Figure 4-6. Measured Heat Load (kW) Applied to the Canister Heaters during the 4-Year Heating Phase. Modeled Heat Indicated with a Solid Line.

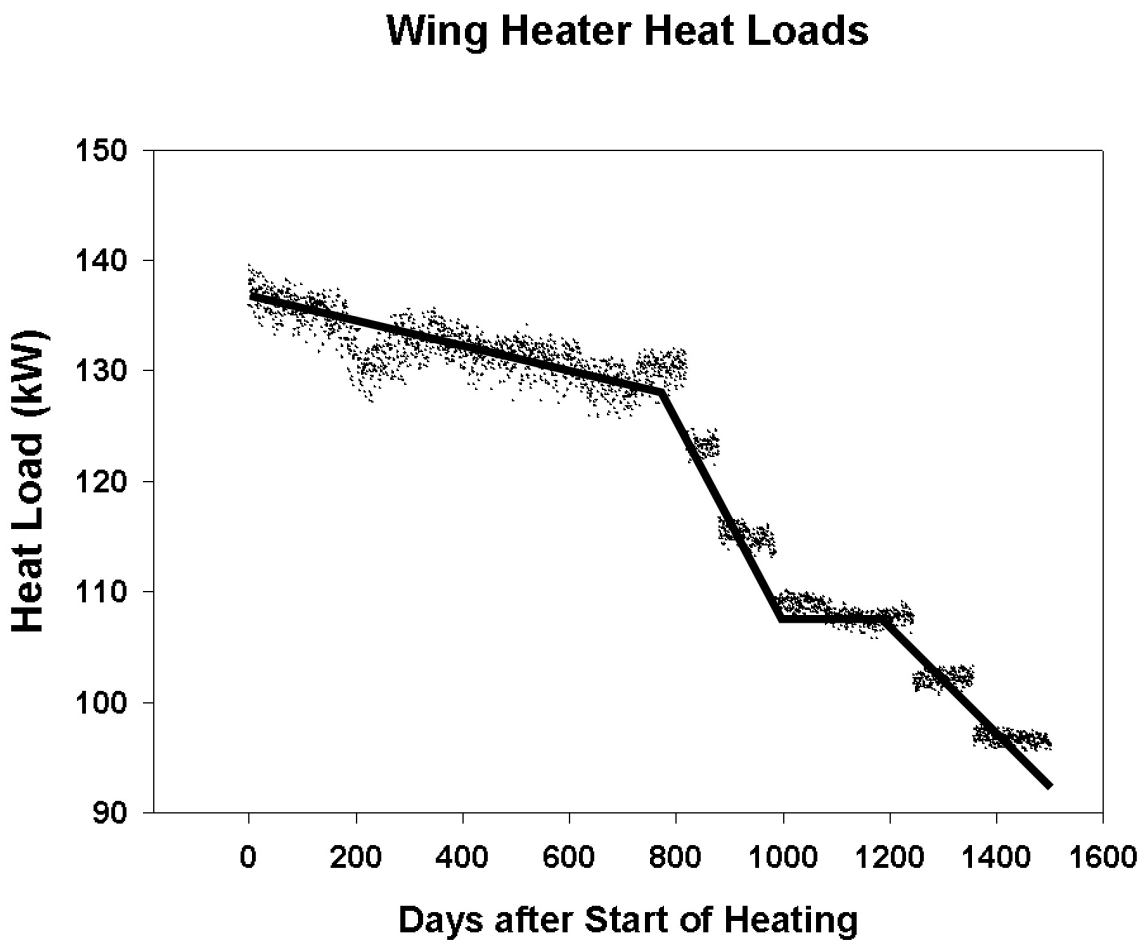

Figure 4-7. Measured Heat Load (kW) Applied to the Wing Heaters during the 4-Year Heating Phase. Modeled Heat Indicated with a Solid Line.

Temperature was directly measured throughout the Drift-Scale Heater Test. Saturation at the Drift-Scale Heater Test is inferred using geophysical methods (i.e., electrical resistivity tomography, ground-penetrating radar, and neutron logging) for the matrix and air permeability tests for the fractures. Inferences from these measurements provide a qualitative measure of saturation at the Drift-Scale Heater Test. Only temperature measurements are used for comparison with thermohydrological simulation results at this time, although inferred saturation measurement techniques may promote a clearer interpretation of the Drift-Scale Heater Test.

Summary results from 6 simulations are reported in this document, although results from only two of the simulations are presented in detail. Major variations among the 6 simulations include: increasing the size of the medium block from 0.40 m [1.31 ft] to 5.0 m [16.4 ft], decreasing the heat load applied to the drift wall by 20 percent, invoking an active fracture model, and including the hydraulic effect of the wing heater borehole. Following is a list of the major features of each simulation:

- Simulation I: small block {0.40 m [1.31 ft]}, high ambient matrix saturation, full drift wall heat load

- Simulation II: small block {0.40 m [1.31 ft]}, high ambient matrix saturation, 20-percent reduction in drift wall heat load

- Simulation III: large block {5.0 m [16.4 ft]}, moderate ambient matrix saturation, full drift wall heat load, wing heater borehole included

- Simulation IV: large block {5.0 m [16.4 ft]}, moderate ambient matrix saturation, 20-percent reduction in drift wall heat load, wing heater borehole included

- Simulation V: small block {0.40 m [1.31 ft]}, moderately high ambient matrix saturation, full drift wall heat load, active fracture model

- Simulation VI: small block {0.40 m [1.31 ft]}, moderately high ambient matrix saturation, 20-percent reduction in drift wall heat load, active fracture model

For ambient matrix saturation, high indicates in excess of 0.99, moderately high indicates approximately 0.98, and moderate means approximately 0.90.

Heat loss through the heated drift bulkhead was quantified as part of an exercise conducted by the U.S. Department of Energy (DOE) to evaluate the impact of the bulkhead on the Drift-Scale Heater Test performance.[2] Conductive heat loss was measured at 6 kW using heat flux meters positioned at 7 locations on the bulkhead. Convective heat loss through the bulkhead was not directly measured but was estimated to be 22 kW using a numerical model. Radiative heat loss was considered by DOE[3] to be included in the conductive heat loss measurement. Conductive (and radiative) heat loss through the bulkhead was incorporated into Simulations II, IV, and V by decreasing the heat load applied to the drift wall by 20 percent. Because the drift wall heat load

---

[2]Wagner, R.A. "Assessment of Heat Loss Through the Drift Scale Test Bulkhead." Interoffice Correspondence (October 21) to M.T. Peters. North Las Vegas, Nevada: CRWMS M&O. 1999.

[3]Ibid.

varied from 52 kW at the onset of the Drift-Scale Heater Test to 38 kW after 4 years of heating, the amount of decreased heat load incorporated into the models varied from 10.4 kW at the start of heating to 7.6 kW at the end of heating during the 4-year simulation—slightly more than the measured values conductive heat loss.

The effect of the wing heater borehole on heat and mass transfer from the rock mass to the drift environment was included in Simulations III and IV by varying the hydraulic properties of the media at the approximate location of the borehole. Permeability was increased in the matrix by a factor of 10,000 and in the fractures by a factor of 1,000 and the relative permeability properties for the matrix were modified to be similar, although not identical, to those of the fractures (i.e., residual saturation of 0.08, m of 0.5, and α of 1.0×10^{-4}), to incorporate the hydraulic effect of the borehole.

Temperatures measured at the Drift-Scale Heater Test were used for comparison with numerical predictions [DTN MO9807DSTSET01.000(113644), MO9810DSTSET02.000(113662), MO9906DSTSET03.000(113673), MO0001SEPDSTPC000(153836), MO0007SEPDSTPC.001(153707), MO0012SEPDSTPC.002(153708), and MO0107SEPDSTPC.003(158321), MO0202SEPDSTTV.001(158320)]. Model results are presented for selected simulations in the following formats:

- Plots of predicted temperatures in Boreholes 158, 160, and 162 at 3 months, 1 year, and 4 years. All three boreholes are located at the middle of the heated drift (Figure 4-8). Borehole 158 is vertically oriented through the crown of the heated drift. Borehole 160 is horizontally oriented through the springline of the heated drift. Borehole 162 is vertically oriented through the base of the heated drift. Predicted temperatures are plotted with temperatures measured in each borehole. Predicted temperatures at the three boreholes are compared to measured temperatures for all six simulations in Figures 4-9 through 4-17. Both fracture and matrix predicted temperatures are included in the figures.

- Contour plots of matrix temperature distribution in the XZ cross section were taken at approximately the middle of the heated drift at 3 months, 1 year, and 4 years. Results from Simulations IV (small block with a 20-percent reduction in drift wall heating and an active fracture model) and VI (large block with a 20-percent reduction in drift wall heating) are presented in Figure 4-18.

- Contour plots of matrix and fracture saturations in the XZ cross section were taken at approximately the middle of the heated drift. Results from Simulations IV (small block with a 20-percent reduction in drift wall heating and an active fracture model) and VI (large block with a 20-percent reduction in drift wall heating) are presented in Figures 4-19 through 4-20.

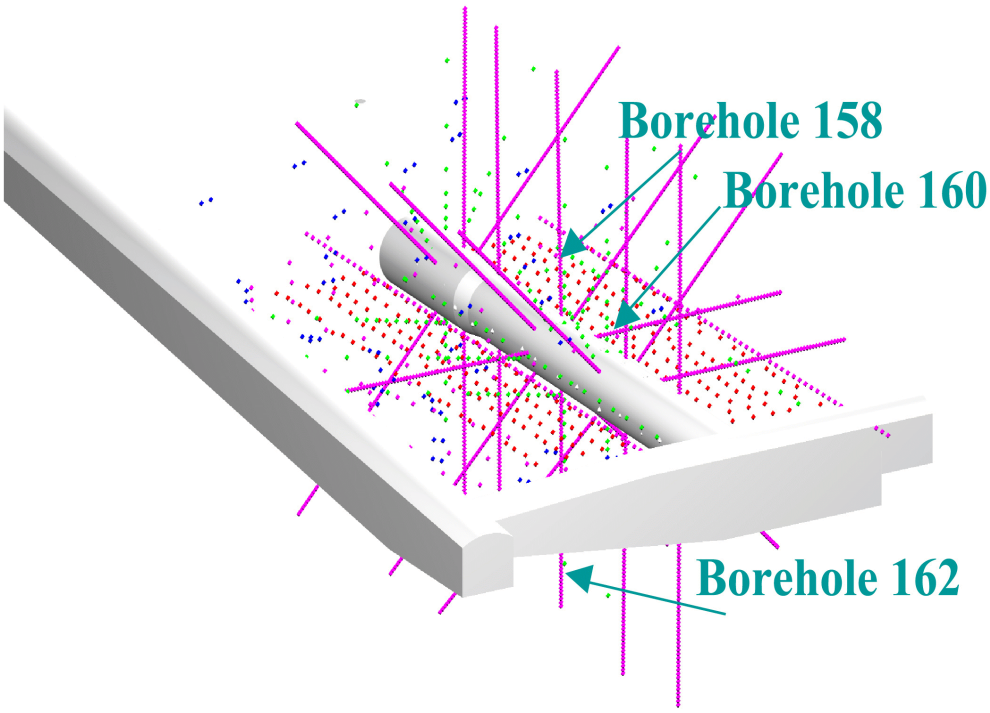

Figure 4-8. Location of Boreholes 158, 160, and 162 Relative to the Heated, Connecting, and Observation Drifts of the Drift-Scale Heater Test

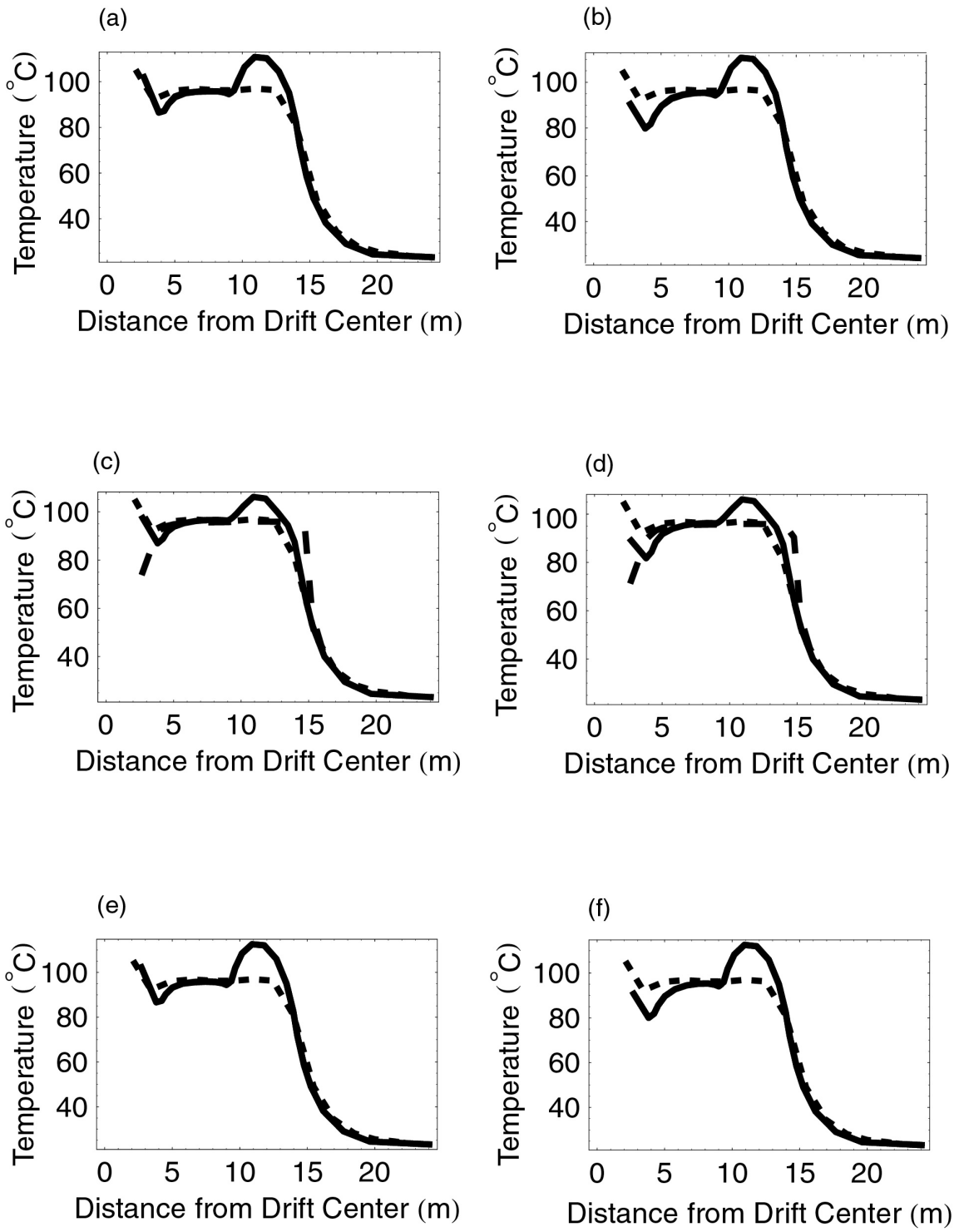

Figure 4-9. Measured Temperature (Short Dashed Line) Versus Simulated Fracture Temperature (Long Dashed Line) and Simulated Matrix Temperature (Solid Line) at Borehole 160 after 3 Months of Heating for Simulations I (a), II (b), III (c), IV (d), V (e), and VI (f). Note the Simulated Fracture and Matrix Temperatures May Appear As One. (Note: 1 m = 3.2808 ft)

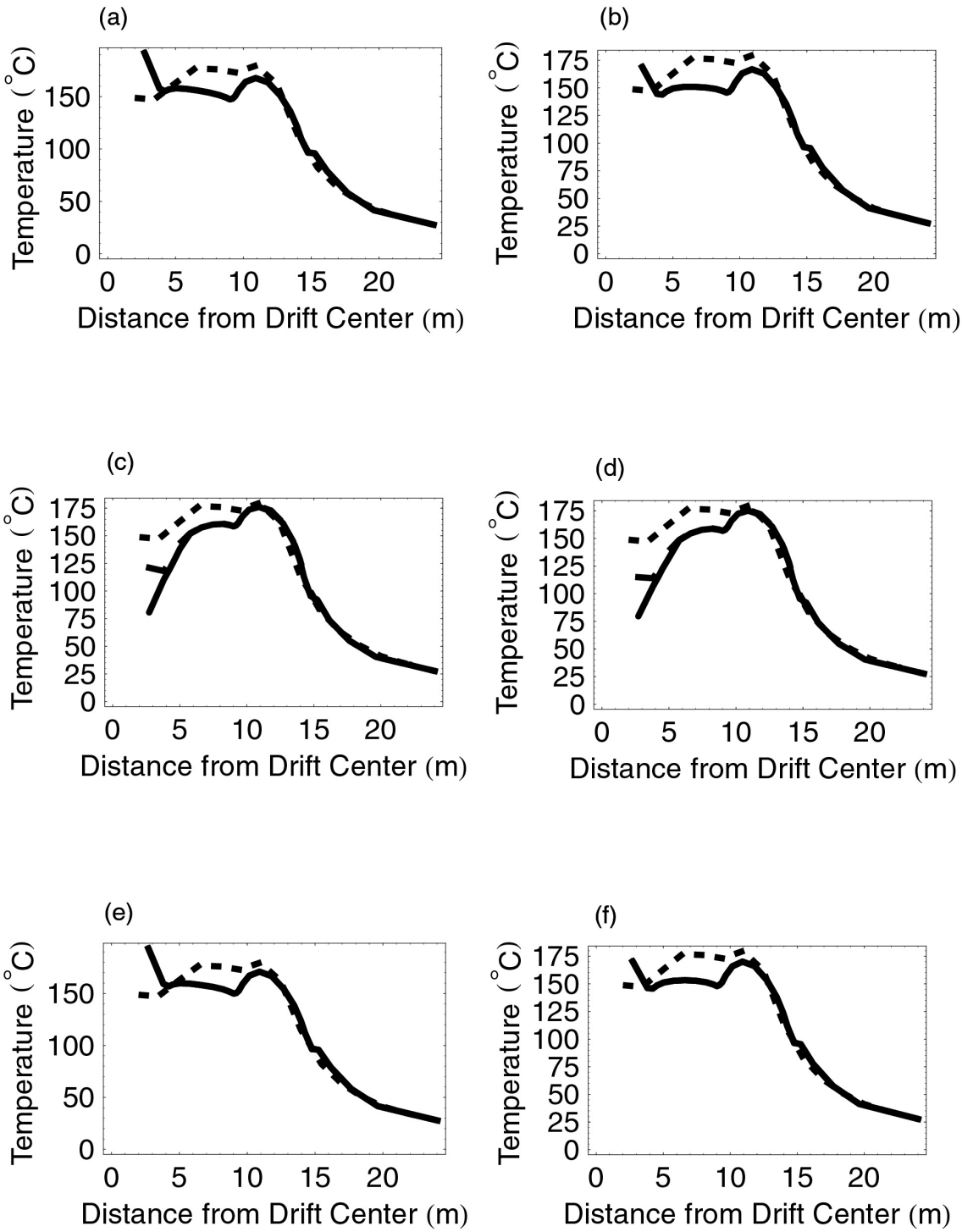

Figure 4-10. Measured Temperature (Short Dashed Line) Versus Simulated Fracture Temperature (Long Dashed Line) and Simulated Matrix Temperature (Solid Line) at Borehole 160 after 1 Year of Heating for Simulations I (a), II (b), III (c), IV (d), V (e), and VI (f). Note the Simulated Fracture and Matrix Temperatures May Appear As One. (Note: 1 m = 3.2808 ft)

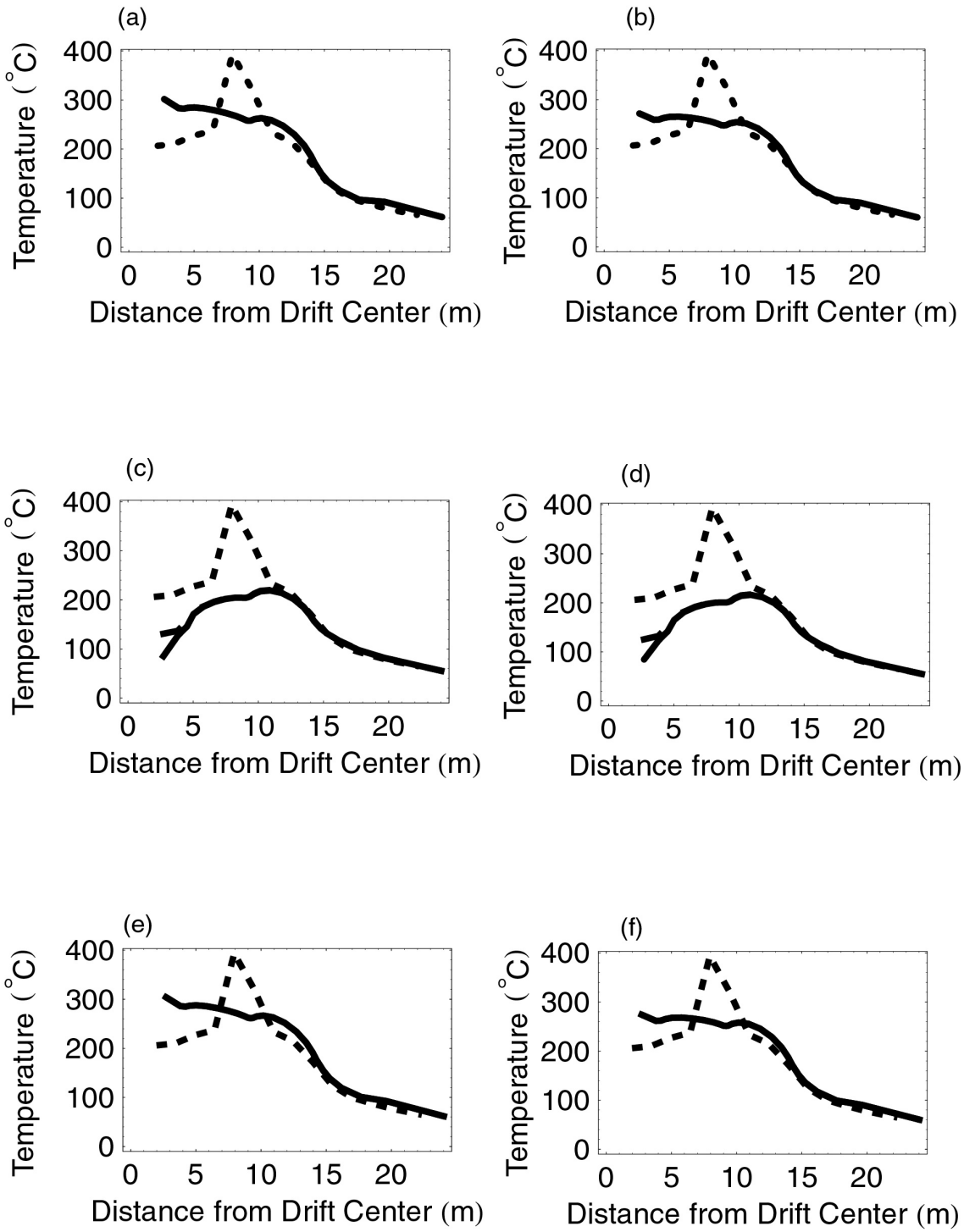

Figure 4-11. Measured Temperature (Short Dashed Line) Versus Simulated Fracture Temperature (Long Dashed Line) and Simulated Matrix Temperature (Solid Line) at Borehole 160 after 4 Years of Heating for Simulations I (a), II (b), III (c), IV (d), V (e), and VI (F). Note the Simulated Fracture and Matrix Temperatures May Appear As One. (Note: 1 m = 3.2808 ft)

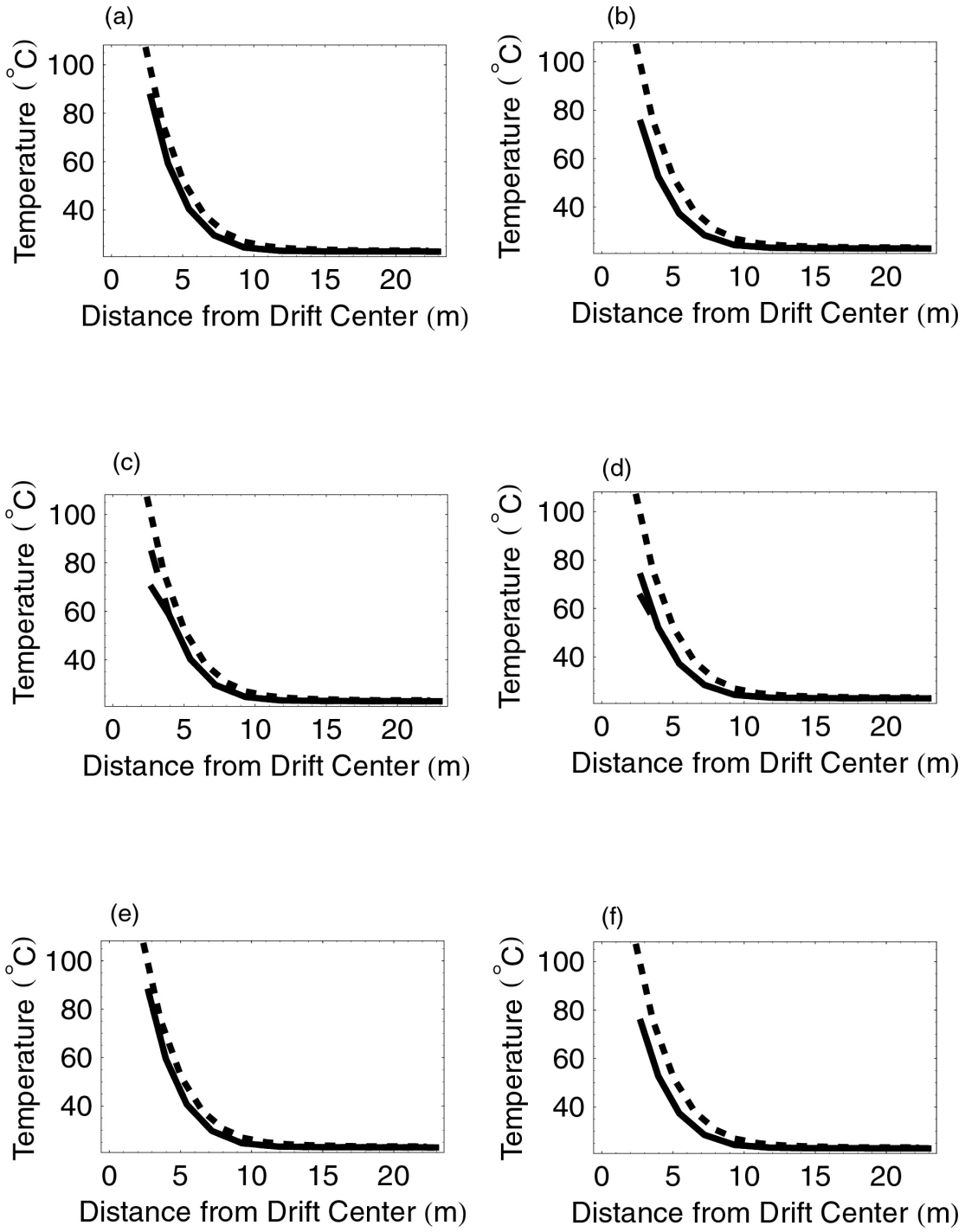

Figure 4-12. Measured Temperature (Short Dashed Line) Versus Simulated Fracture Temperature (Long Dashed Line) and Simulated Matrix Temperature (Solid Line) at Borehole 158 after 3 Months of Heating for Simulations I (a), II (b), III (c), IV (d), V (e), and VI (f). Note the Simulated Fracture and Matrix Temperatures May Appear As One. (Note: 1 m = 3.2808 ft)

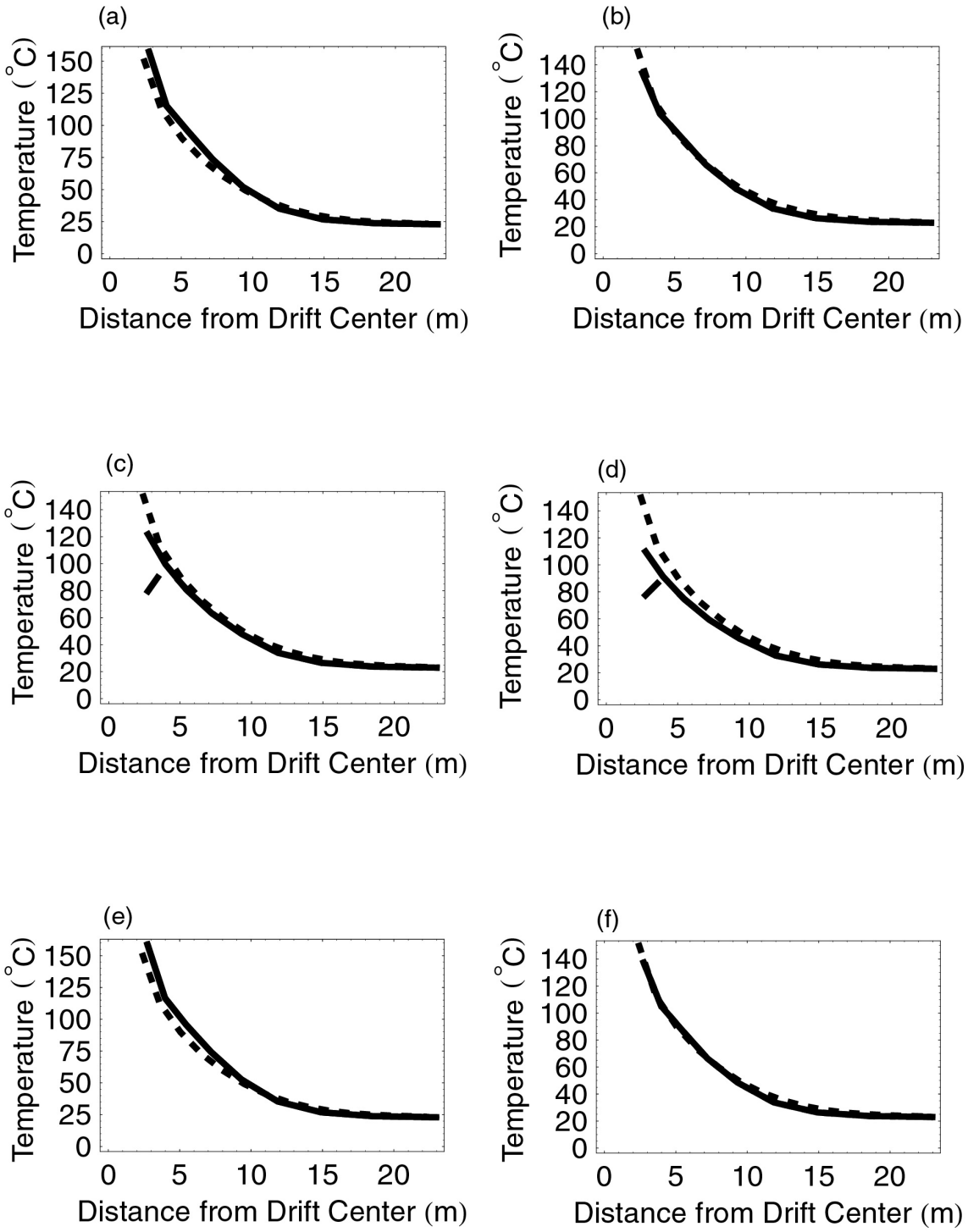

Figure 4-13. Measured Temperature (Short Dashed Line) Versus Simulated Fracture Temperature (Long Dashed Line) and Simulated Matrix Temperature (Solid Line) at Borehole 158 after 1 Year of Heating for Simulations I (a), II (b), III (c), IV (d), V (e), and VI (F). Note the Simulated Fracture and Matrix Temperatures May Appear as One. (Note: 1 m = 3.2808 ft)

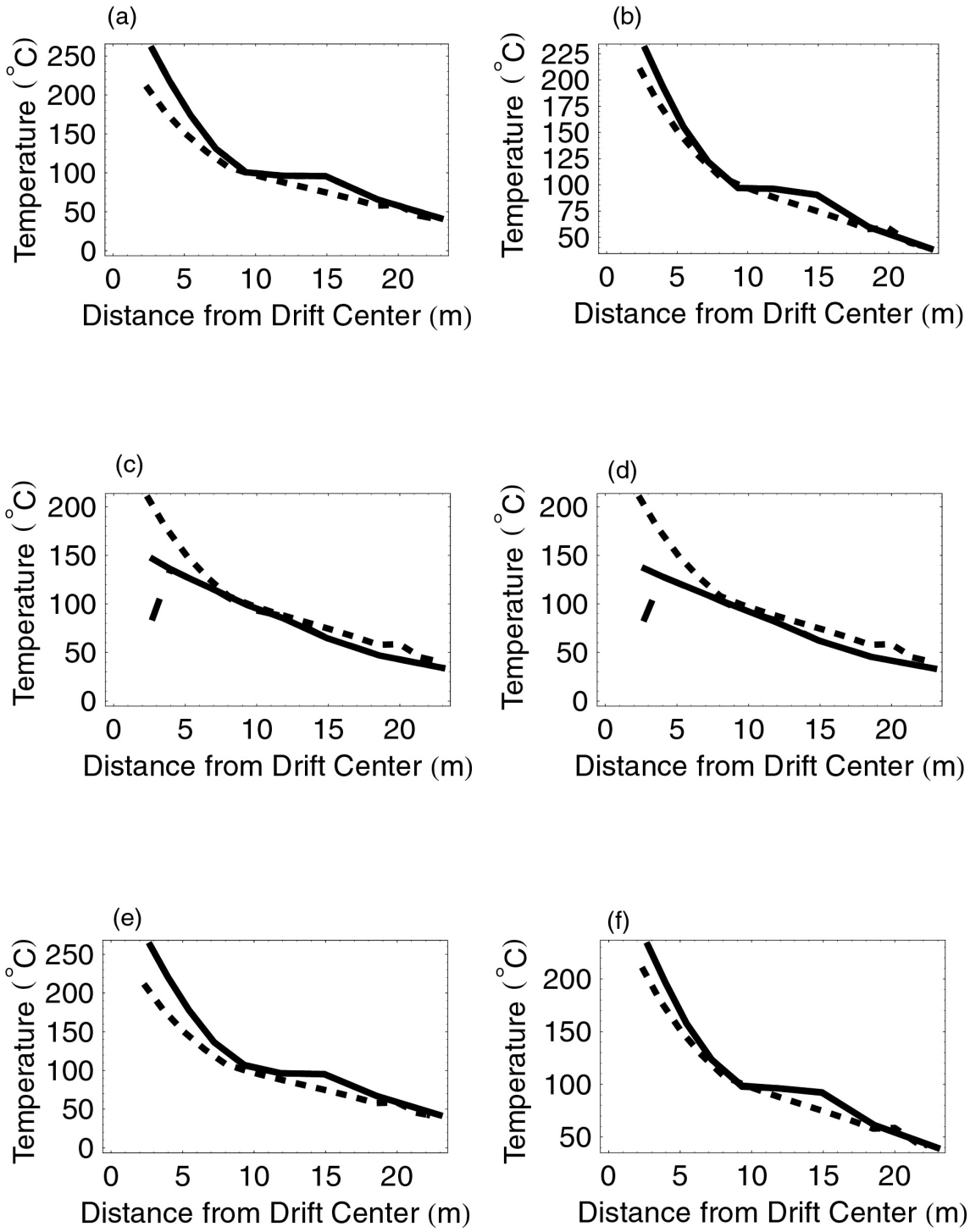

Figure 4-14. Measured Temperature (Short Dashed Line) Versus Simulated Fracture Temperature (Long Dashed Line) and Simulated Matrix Temperature (Solid Line) at Borehole 158 after 4 Years of Heating for Simulations I (a), II (b), III (c), IV (d), V (e), and VI (f). Note the Simulated Fracture and Matrix Temperatures May Appear as One. (Note: 1 m = 3.2808 ft)

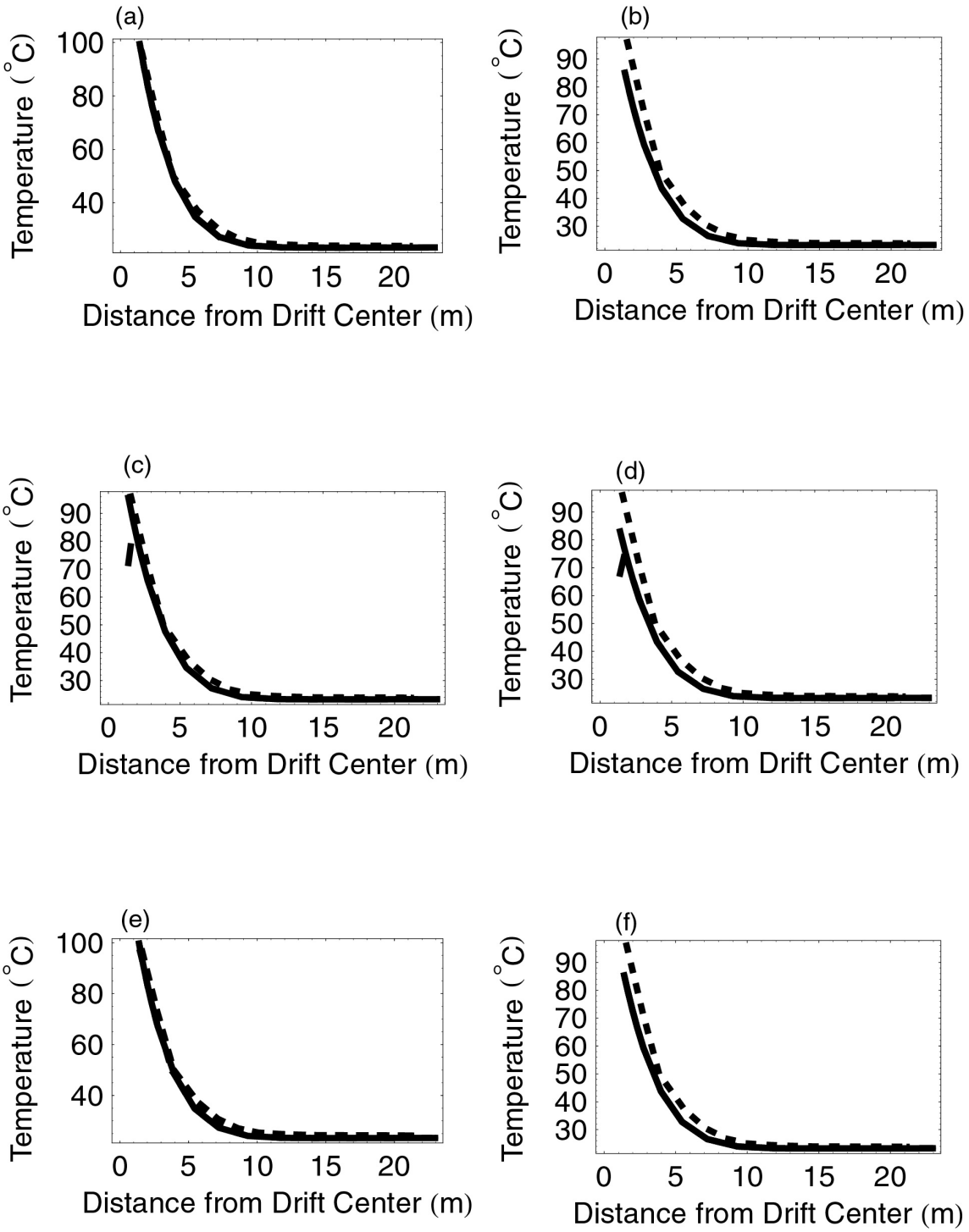

Figure 4-15. Measured Temperature (Short Dashed Line) Versus Simulated Fracture Temperature (Long Dashed Line) and Simulated Matrix Temperature (Solid Line) at Borehole 162 after 3 Months of Heating for Simulations I (a), II (b), III (c), IV (d), V (e), and VI (f). Note the Simulated Fracture and Matrix Temperatures May Appear As One. (Note: 1 m = 3.2808 ft)

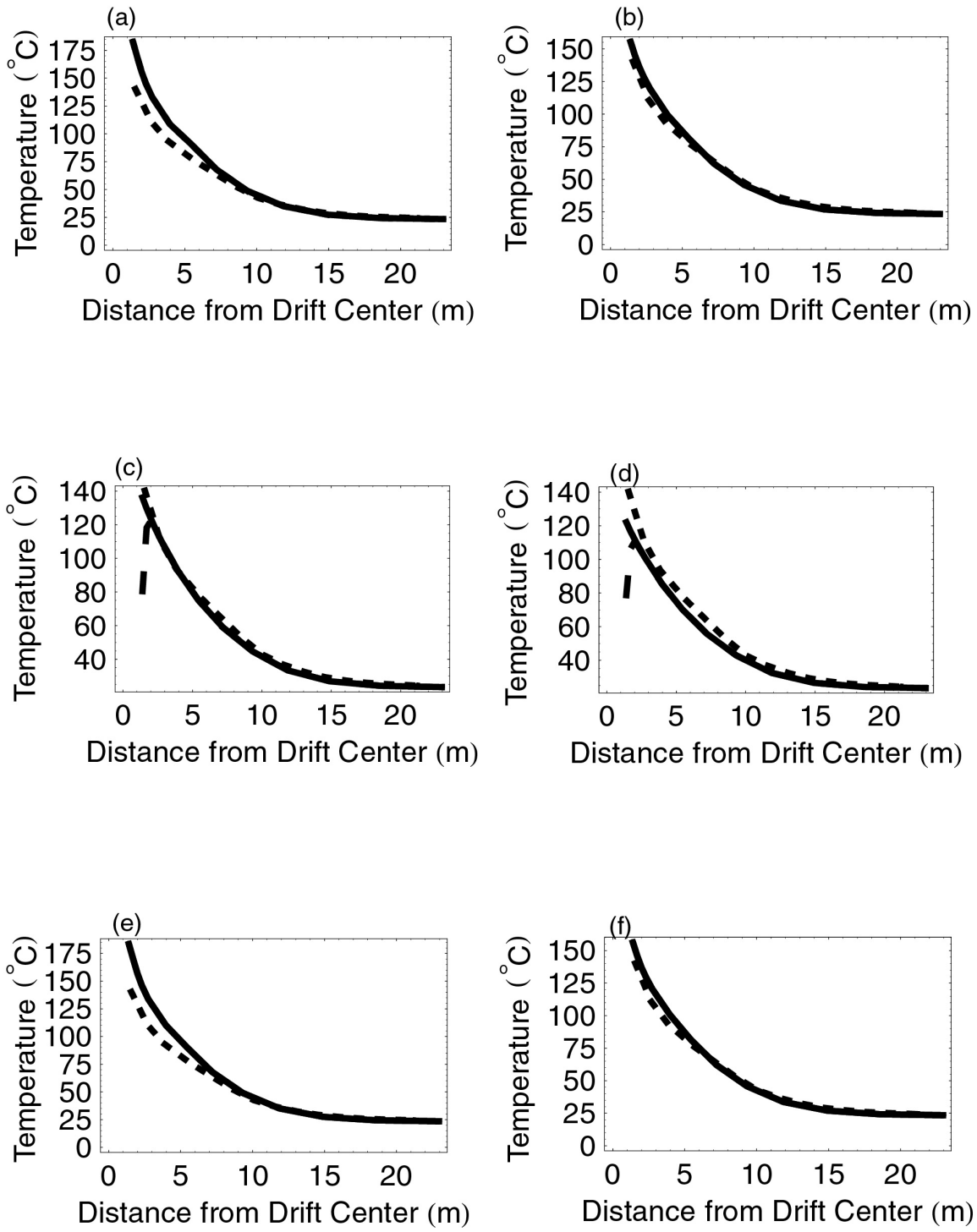

Figure 4-16. Measured Temperature (Short Dashed Line) Versus Simulated Fracture Temperature (Long Dashed Line) and Simulated Matrix Temperature (Solid Line) at Borehole 162 after 1 Year of Heating for Simulations I (a), II (b), III (c), IV (d), V (e), and VI (f). Note the Simulated Fracture and Matrix Temperatures May Appear As One. (Note: 1 m = 3.2808 ft)

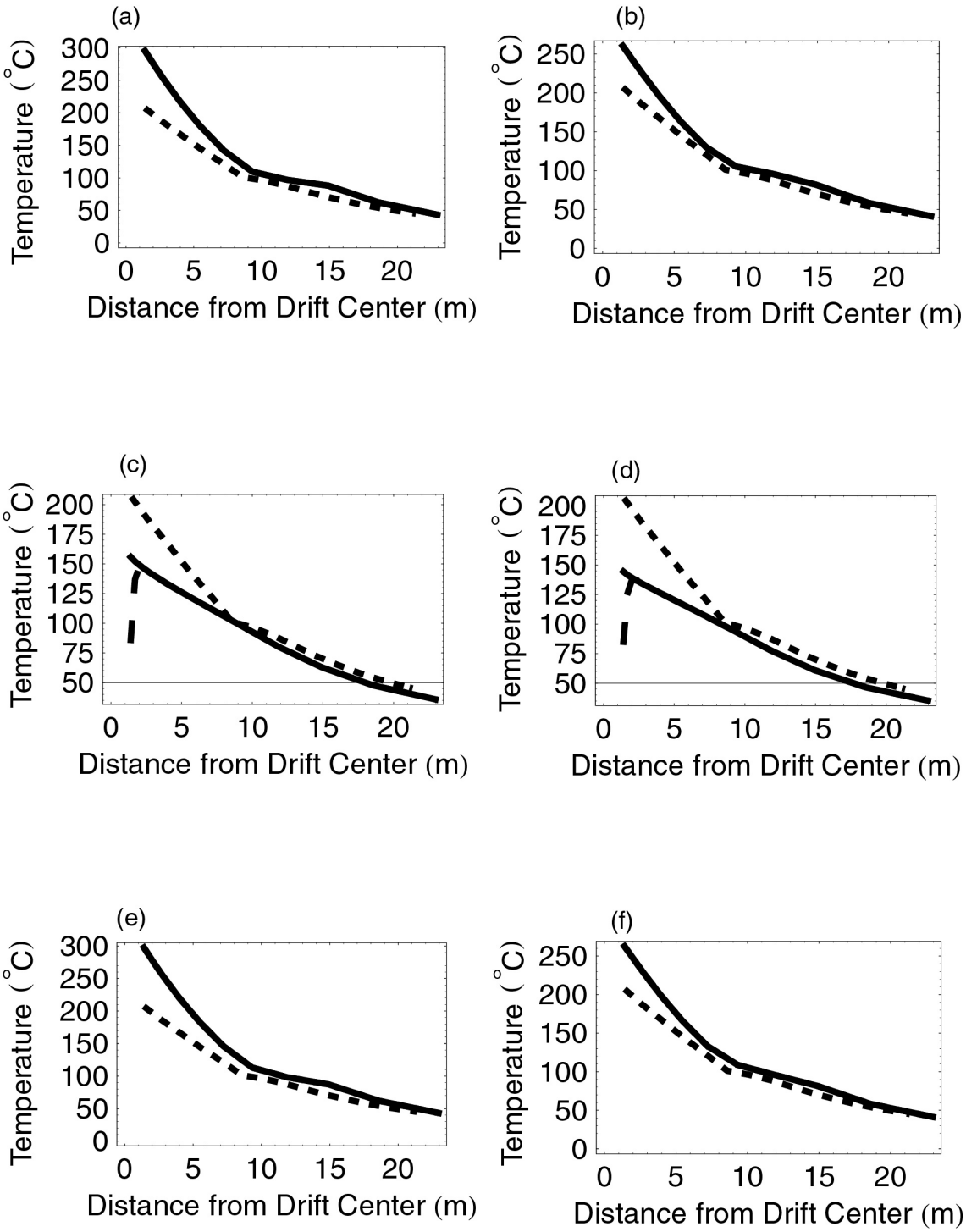

Figure 4-17. Measured Temperature (Short Dashed Line) Versus Simulated Fracture Temperature (Long Dashed Line) and Simulated Matrix Temperature (Solid Line) at Borehole 162 after 4 Years of Heating for Simulations I (a), II (b), III (c), IV (d), V (e), and VI (f). Note the Simulated Fracture and Matrix Temperatures May Appear As One. (Note: 1 m = 3.2808 ft)

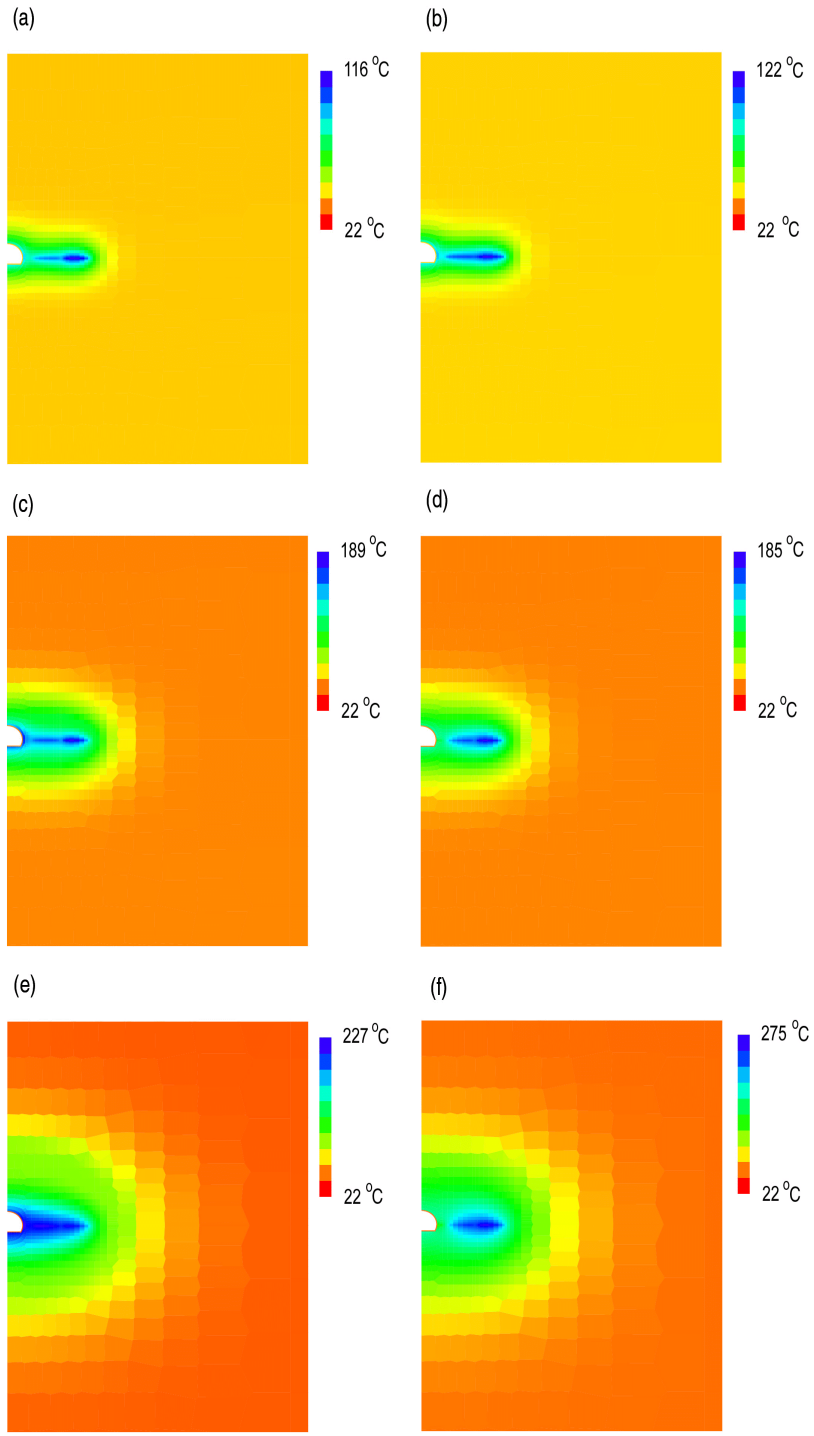

Figure 4-18. Contour Plots of Matrix Temperature after 3 Months, 1 Year, and 4 Years of Heating Predicted by Simulations IV [(a), (c), (e)] and VI [(b), (d), (f)]

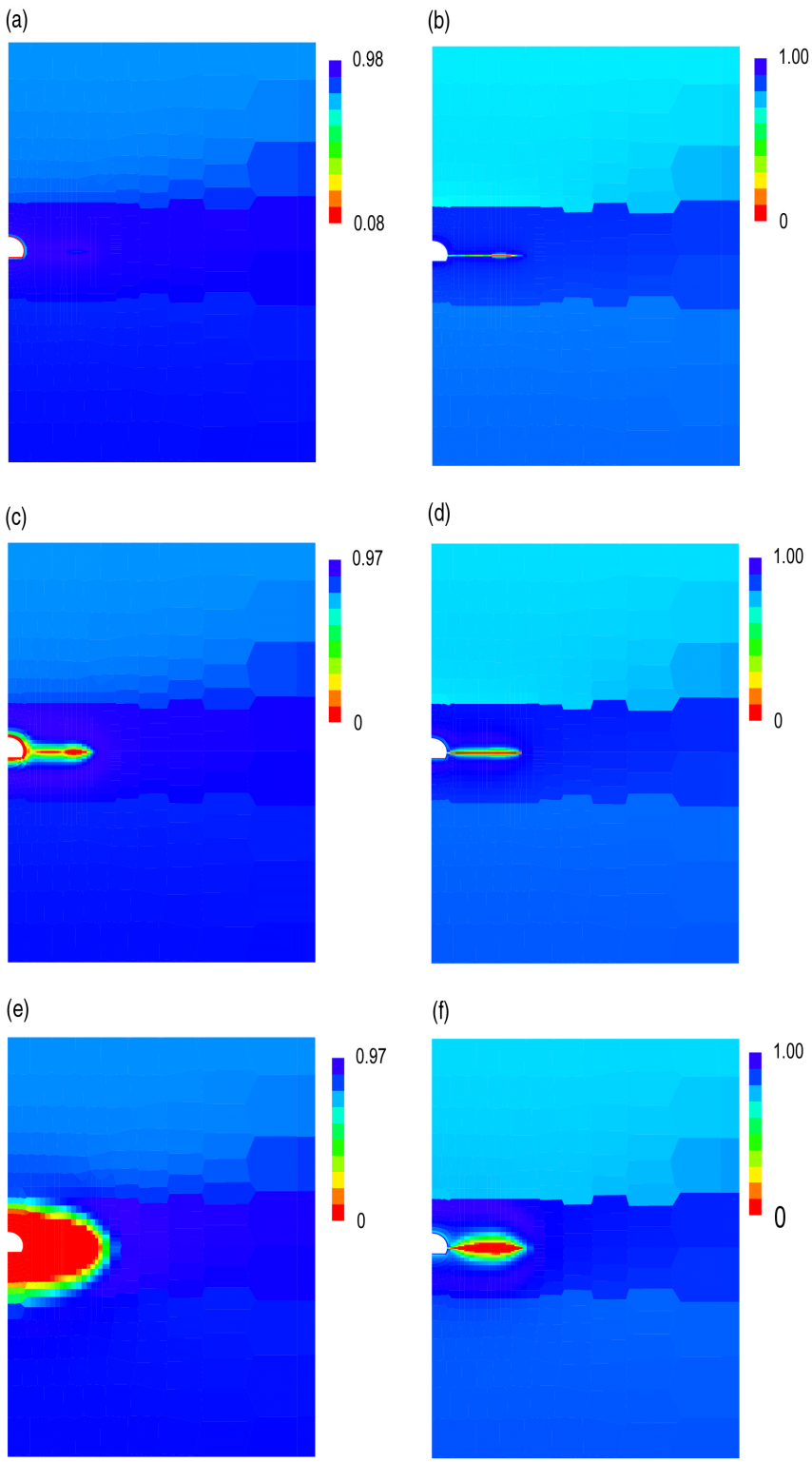

Figure 4-19. Contour Plots of Matrix Saturation after 3 Months, 1 Year, and 4 Years of Heating Predicted by Simulations IV [(a), (c), (e)] and VI [(b), (d), (f)]

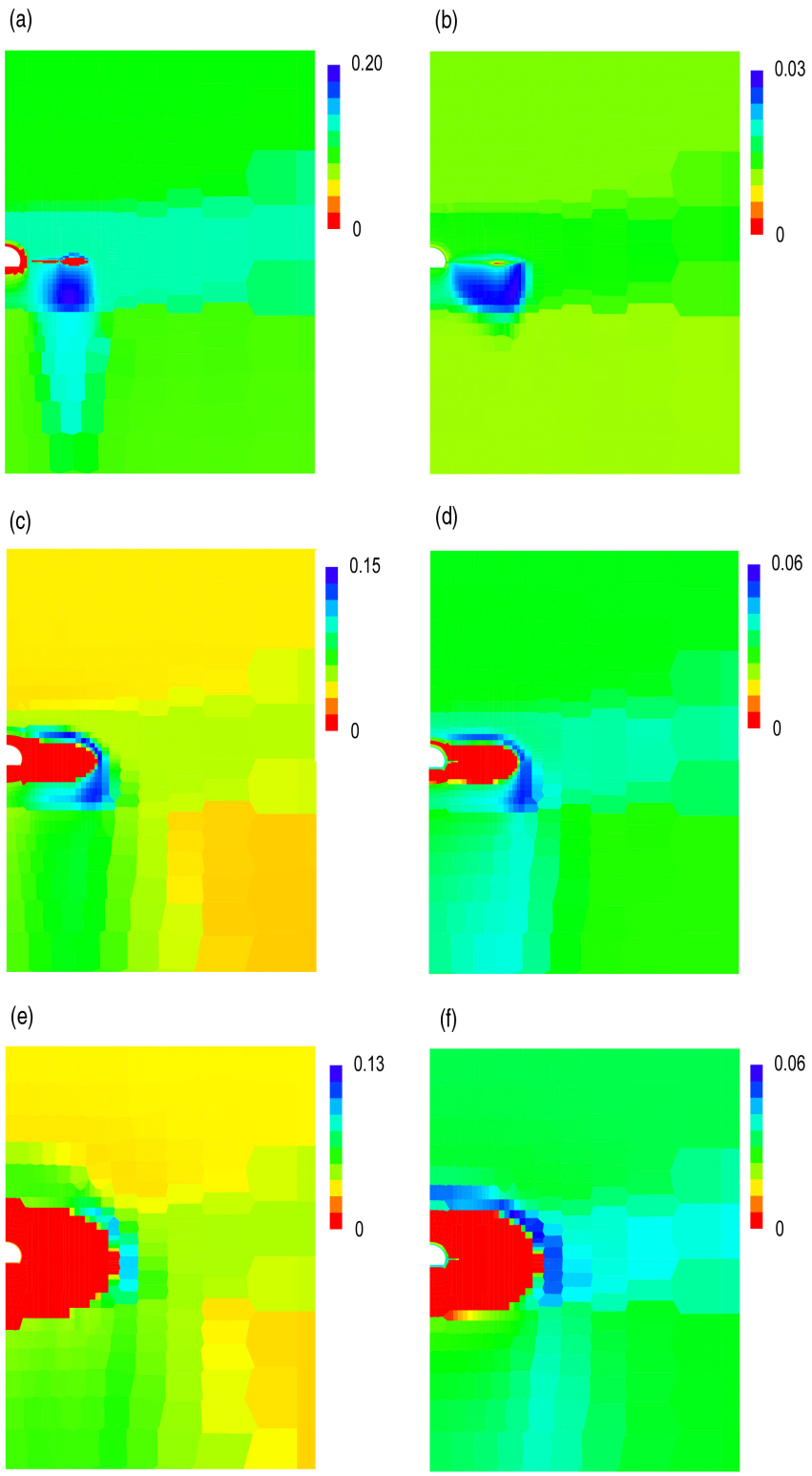

Figure 4-20. Contour Plots of Fracture Saturation after 3 Months, 1 Year, and 4 Years of Heating Predicted by Simulations IV [(a), (c), (e)] and VI [(b), (d), (f)]

4.5.3 Model Results

Specific observations are listed below, followed by general observations. Comparison of predicted temperatures to temperatures measured at Boreholes 158, 160, and 162 provides the best quantitative measure of the success of the model to replicate heat and mass transfer at the Drift-Scale Heater Test. A feature of particular interest in temperatures is the formation of a heat pipe. Temperatures maintained at boiling for some distance are taken as evidence of a heat pipe. The presence of a heat pipe is of interest because a heat pipe acts as a particularly efficient heat transfer mechanism. A heat pipe may be an indication of a reflux halo, which, when located above the heaters, could be a source for water flowing downward toward the heaters.

- Measured temperatures in Borehole 160 (parallel to and above the wing heaters) did not exceed boiling until after 3 months (Figure 4-12). Conversely, all simulations predicted temperatures at locations above the outer wing heater that were in excess of boiling {i.e., approximately 110 °C [230 °F]} by 3 months. This consistent difference between measured temperatures and the simulation results may be an issue related to the resolution of gridding near the heat source and the location of Borehole 160. Alternatively, temperatures measured in Borehole 160 above the inner wing heater are similar to those over the outer wing heater, a relationship not observed in any simulation results (Figures 4-12 through 4-14). This relationship is not consistent with the 40/60 ratio of heat loading assigned to the 2 wing heaters in the models.

- A small heat pipe was predicted immediately beyond the end of the outer wing heater in Borehole 160 at 1 year in all 6 simulations (Figure 4-13). There was no indication of a heat pipe at this location in the simulations at 4 years. No heat pipe was observed in the measured temperatures at this location at either 1 or 4 years (Figures 4-13 and 4-14).

- No appreciable difference between matrix and fracture temperatures was predicted for small block simulations. Conversely, appreciable differences in matrix and fracture temperatures were predicted proximal to the heat source at all three boreholes at all three times in large block simulations. Fracture temperatures were significantly depressed relative to predicted matrix temperatures at nodes located on the drift wall for large block simulations, therefore fracture temperatures at the drift wall were consistently held to approximately 80 °C [176 °F]. It is believed that these fracture temperatures are an artifact of the large block size and the particular attributes assigned to the drift wall boundary, and consequently, the predicted fracture temperatures at the drift wall are not physically meaningful.

- For times of 1 year and greater, small block simulations, even with a 20-percent reduction in the drift-wall heat load, had temperatures generally greater than measured temperatures above and below the heated drift (Figures 4-10, 4-11, 4-16, and 4-17). Conversely, predicted temperatures at the heated drift springline and above the inner wing heater (Borehole 160) were less than those observed for the same time period (Figures 4-12 and 4-13). This temperature discrepancy suggests that a uniform heat load applied to the drift wall may not be consistent with actual heat loads that were experienced during the 4-year heating phase.

- Large-block model simulation temperatures were less than measured temperatures with the exception of Borehole 160 temperatures over the outer wing heater at 3 months.

- The large temperature spike measured at 4 years in Borehole 160 near the outer wing heater {i.e., 400 °C [752 °F]} was not replicated in any simulations (Figure 4-14). This anomalously high temperature was measured at several temperature sensors and is not believed to be a measurement or instrument error. The high temperature is attributed to geologic heterogeneity, possibly a zone of high fracture density; however, the exact cause for these anomalously high observed temperatures is not identified.

- A heat pipe was indicated in the measured temperatures from Borehole 162 approximately 9 to 11 m [29.5 to 36.1 ft] below the heater drift center at 4 years (Figure 4-17). The small block simulations predicted heat pipes in approximate agreement with the observations. Neither of the large block simulations predicted a heat pipe in Borehole 162.

- No heat pipe was observed in Borehole 158 at any time (Figures 4-9 through 4-11). A prominent {approximately 6 to 7 m [19.7 to 23.0 ft] long} heat pipe was predicted above the heater drift by the small block simulations at 4 years (Figure 4-11).

- Inclusion of the hydraulic properties of the wing heater borehole did not have a significant effect on heat and mass transfer in the large block simulations, with the exception of those elements assigned borehole properties (Figures 4-18 through 4-20).

Following are general observations of the model results evaluations.

- The active fracture model decreased ambient saturations for the small block models from saturations in excess of 0.99 to approximately 0.98. These saturations are still greater than those measured (approximately 0.92).

- The active fracture model had no appreciable effect on predicted temperatures compared to similar models with no active fracture model.

- In the differences between measured and predicted temperatures at the three boreholes compared, small block models outperformed large block models by providing smaller differences for most comparisons.

- The small block model with the drift wall heat load reduced by 20 percent appeared to predict temperatures slightly closer to observed temperatures than the small block simulation with full drift wall heat load. Nonetheless, relatively large discrepancies between predicted and measured temperatures at the drift wall suggest that additional heat load modification (i.e., nonuniform heat loadings) would be required to better approximate the actual canister heat load by using heat loads applied to the drift wall.

- There was a large difference between matrix saturations predicted by the small and large block models (Figure 4-19). At 4 years, a significantly larger dryout zone {i.e., 4 m [13.1 ft] both above and below the heated drift and wing heaters} was predicted in the small block model compared to the large block model {with a total dryout thickness of 2–3 m [6.6–9.8 ft]}.

- The extent of the dryout zone predicted at 4 years was similar in all simulations {approximately 5 m [16.4 ft] above and below the heater drift and slightly beyond the far end of the outer wing heater} (Figure 4-20). All simulations predicted that a significant amount of the vaporized water would condense in the fractures below the wing heaters compared to above the wing heaters. Greater drainage through the fractures to regions below the Drift-Scale Heater Test horizon was predicted by the small block simulations, whereas greater ponding in the fractures above the Drift-Scale Heater Test horizon was predicted by the large block simulations.

5 DISCUSSION AND SUMMARY

Modeling is an important part of assessing and developing confidence in evaluating the safety of a potential geologic repository at Yucca Mountain, Nevada. The Drift-Scale Heater Test at Yucca Mountain has been used to provide a basis to assess the capability of the thermohydrological codes to simulate complex thermohydrological processes. This report was prepared to document the results of an enhanced numerical model that was developed to independently evaluate MULTIFLO, a model used by the Nuclear Regulatory Commission to support its high-level waste repository safety program, and the capability of MULTIFLO to evaluate various thermohydrological conceptual models and the effects of property assignments. The numerical model was enhanced from previous models (Green, et al., 2000, 2001) by increasing the dimensionality from two to three and by incorporating more realistic boundary conditions at the drift wall. Results from the MULTIFLO analyses can be compared with results from other thermohydrological codes to evaluate the ability of the code to simulate heat and mass transfer through partially saturated fractured rock.

The enhanced three-dimensional model used an unstructured grid to represent the Drift-Scale Heater Test. Two vertical planes of symmetry allowed modeling only one-fourth of the entire Drift-Scale Heater Test domain. The fractured rock medium was represented with a dual (matrix and fracture) continuum conceptual model. The effects of block size {0.4 m [1.31 ft] versus 5.0 m [16.4 ft]}, reduction in the heat load applied to the drift wall, inclusion of an active fracture model, and hydraulic inclusion of the wing heater borehole in the test medium were evaluated in this study. Model predictions of temperature were compared with Drift-Scale Heater Test temperature measurements after 3 months, 1 year, and 4 years of the heating phase to perform the evaluations.

Combinations of property values and boundary conditions other than those used in these analyses can also predict reasonable ambient matrix saturations. Predicting an appropriate ambient saturation using a particular model does not in itself ensure that either the conceptual model or the assigned model input values are appropriate, or even acceptable, representations of the Drift-Scale Heater Test. Additionally, the question remains whether the documented ambient saturation values are representative of the Drift-Scale Heater Test environment prior to heating. Sources of uncertainty include (i) what was the effect of drilling and excavation on the collected rock samples, (ii) how were the rock samples preserved after collection to prevent dryout, and (iii) do the limited number of rock samples collected and measured for saturation provide a sufficient representation of actual conditions. This uncertainty limits the level of confidence in the results of the simulations.

An increase in the model block size from 0.40 [1.31] to 5.0 m [16.4 ft] allowed relatively large infiltration rates {i.e., 3.0 mm/yr [0.001 ft/yr]} while maintaining a moderate ambient matrix saturation (i.e., approximately 0.90). Conversely, a relatively low infiltration rate {i.e., 0.07 mm/yr [0.0002 ft/yr]} was required to attain a 0.90 matrix saturation for the small block in the standard case. In this case, an infiltration rate of 3.0 mm/yr [0.001 ft/yr] resulted in an ambient matrix saturation in excess of 0.99. Modifying the standard model {i.e., small block model and infiltration of 3.0 mm/yr [0.001 ft/yr]} by invoking an active fracture model resulted in an ambient matrix saturation of approximately 0.98. The active fracture model therefore reduced the ambient saturation of the matrix for the small block simulations with relatively large infiltration {i.e., 3.0 mm/yr [0.001 ft/yr]}. This apparent enigma among block size, infiltration, and saturation was also observed in previous two-dimensional simulations (Green, et al., 2000, 2001). These

results indicate that model dimensionality (i.e., either two or three dimensions) is not a source of this enigma. Additional evaluations of the active fracture model may help resolve this enigma. However, at this time, model results from these simulations do not significantly reduce uncertainty in the values assigned to boundary conditions at Yucca Mountain (i.e., surface infiltration rates).

The active fracture model had no appreciable effect on heat and mass transfer during the 4 years of heating. This lack of effect during heating is because most mass (water) movement is from the matrix to the fracture as water is vaporized; then it flows through the fracture as vapor and liquid. The active fracture model only reduces the relative permeability for mass transfer from the fracture to the matrix and not from the matrix to the fracture.

Comparison of model results based on two block sizes can be interpreted to support the premise that the appropriate block size may be between the two block sizes evaluated in this study {i.e., between 0.40 m [1.31 ft] and 5.0 m [16.4 ft]}, although these trends are not universally true. For example, small block simulations predict temperatures that are slightly less than measured temperatures at 3 months and 1 year in at least part of Borehole 160.

Irrespective of particular attributes, none of the models accurately reflected temperatures near the heated drift. In particular, model temperatures were too low at the springline at early time (i.e., 3 months) for the small block simulations but too high at late times for the same simulations. Predicted temperatures at both the drift crown and floor are too high, particularly at late times, even with a 20-percent reduction in the drift wall heat load. This disparity suggests that conductive and radiative heat losses from the canisters through the bulkhead may not be adequately represented as a constant, uniform reduction of the heat load applied to the drift wall. This feature is understandable given the transient factors that contributed to application of heat loads and removal of heat from the connecting drift during the heating phase.

Insight into coupled thermohydrological processes gained in these analyses is relevant to Technical Agreements TEF.2.01, TEF.2.08, TEF.2.10, and TEF.2.11. The effect of heat and mass losses through the bulkhead during the Drift-Scale Heater Test (TEF.2.01) was analyzed using this enhanced numerical model of the Drift-Scale Heater Test. A constant pressure boundary condition was applied to the drift wall. This boundary condition allowed mass (as water vapor) and heat (as enthalpy) to exit the modeled volume (i.e., through the bulkhead). Heat loss through the bulkhead by conduction and radiation was incorporated into the model by reducing the canister heat load (applied to the drift wall) by 20 percent. Inconsistent agreement between measured and predicted temperature near the drift wall suggests that heat loss through the bulkhead is not completely represented by the manner in which the canister heat load was applied to the model and the method used to represent conductive and radiative heat loss through the bulkhead.

Penetration of the boiling isotherm by water refluxing down fractures, as represented by the O.M. Phillips analytical solution (Phillips, 1996), (TEF.2.08) was not directly addressed in these analyses. Nonetheless, accurate prediction of the extent of drying and the formation of heat pipes in partially saturated fractured rock in the presence of heating is imperative if the refluxing phenomenon is to be adequately understood and predicted. Analysis of the Drift-Scale Heater Test has provided additional insight into the coupled thermohydrological processes that control drying and heat pipe formation, but uncertainty still exists. In particular, the reason for the absence of refluxing water down fractures and into the drift at the Drift-Scale Heater Test cannot

be unequivocally explained. The absence of refluxing at the Drift-Scale Heater Test may be due to a sufficiently extensive dry-out zone; however, this absence may also be due to heat and mass losses through the bulkhead. Insufficient confidence in the way the effects of the bulkhead were incorporated into the model prohibits resolving this dilemma. In the absence of measured heat and mass loss rates through the bulkhead, results from the Drift-Scale Heater Test cannot be used to ascertain why refluxing was not observed during the 4-year heating phase. As a consequence, these analyses do not increase confidence in the simulations used to predict the potential for refluxing at a potential Yucca Mountain repository. As an additional consequence, the reflux modules used in the TPA Version 4.0 code (Mohanty, et al., 2002) could not be evaluated or enhanced, nor could the confidence in the modules be increased, using results from these analyses. The U.S. Department of Energy will need to address this limitation in order to close Technical Agreement TEF.2.01.[1]

The effect of variability of select thermodynamic variables on heat and mass transfer was assessed (TEF.2.11). Thermodynamic variables investigated were matrix/fracture interaction properties, thermal conductivity properties assigned to the wing heater boreholes and the drift wall, and block dimensions. Additional thermodynamic properties investigated as part of earlier Drift-Scale Heater Test analyses included fracture permeability and thermal conductivity of the rock mass. These properties were investigated because of their potentially significant impact on heat and mass transfer in fractured rock.

Property values used in this enhanced thermodynamic model were taken from the most current listing of calibrated properties (TEF.2.11) (CRWMS M&O, 2001).

Generation of the three-dimensional Drift-Scale Heater Test model with enhanced boundary conditions at the drift wall permitted more realistic simulation of the actual test results compared with earlier modeling results (Green, et al., 2000, 2001). Nonetheless, differences between predicted and measured temperatures near the drift wall suggest that the uniform application of a heat load to the drift wall used in this model may not be appropriate. Applying the heat load directly to the drift wall neglects the effect of in-drift heat transfer processes. It is not anticipated that all thermohydrological model uncertainty will be reduced to a desirable level solely by using results from the Drift-Scale Heater Test. In particular, uncertainty with regard to heat and mass losses through the bulkhead cannot be adequately resolved using numerical simulation. The more highly controlled heater test proposed for the cross drift at Yucca Mountain, the Cross-Drift Thermal Test, may provide sufficient confirmatory test results to demonstrate the adequacy to the DOE conceptual models.

[1]Technical Agreements TEF.2.01 and TEF.2.08 were open at the time this report was delivered to U.S. NRC in September 2002, but were closed at the time this report was released in September 2007.

6 REFERENCES

Birkholzer, J.T. and Y.W. Tsang. "Modeling the Thermal-Hydrologic Processes in a Large-Scale Underground Heater Test in Partially Saturated Fractured Tuff." *Water Resources Research*. Vol. 36, No. 6. pp. 1,431–1,447. 2000.

———. "Pretest Analysis of the Thermal-Hydrological Conditions of the ESF Drift-Scale Test." Earth Sciences Division Level 4 Milestone Report SP9322M4. Berkeley, California: Lawrence Berkeley National Laboratory. 1997.

Blair, S., T. Buscheck, L. DeLoach, W. Lin, and A. Ramirez. "Single Heater Test Final Report." UCRL–ID–131491. Livermore, California: Lawrence Livermore National Laboratory. 1998.

Bodvarsson, G.S. and T.M. Bandurraga. "The Site-Scale Unsaturated Zone Model of Yucca Mountain, Nevada, for the Viability Assessment." LBNL–40376. Berkeley, California: Lawrence Berkeley National Laboratory. 1997.

Brechtel, C.E., G. Lin, E. Martin, and D.S. Kessel. "Geochemical Characterization of the North Ramp of the Exploratory Studies Area." SAND95–0488. Albuquerque, New Mexico: Sandia National Laboratories. 1995.

Brooks, R.H. and A.T. Corey. "Properties of Porous Media Affecting Fluid Flow." *Journal of Irrigation and Drainage Engineering*. Vol. 92. pp. 61–88. 1966.

CRWMS M&O. "Multiscale Thermohydrologic Model." ANL–EBS–MD–000049. Rev. 00 ICN 02. North Las Vegas, Nevada: CRWMS M&O. 2001.

———. "Total System Performance Assessment–Viability Assessment (TSPA-VA) Analyses Technical Basis Document." B00000000–01717–4301. Rev. 01. Las Vegas, Nevada: TRW Environmental Safety Systems, Inc. 1998.

Green, R.T., M.E. Hill, and S. Painter. "Progress Report for DECOVALEX III Task 2: Numerical Simulation of the Drift-Scale Heater Test at Yucca Mountain." San Antonio, Texas: CNWRA. 2001.

Green, R.T., D. Hughson, S. Painter, and M.E. Hill. "Evaluation of the Drift-Scale Heater Test Thermal-Hydrological Conceptual Model Data and U.S. Department of Energy Thermal Test Results—Status Report." San Antonio, Texas: CNWRA. 2000.

Hirschfelder, J.O., C.F. Curtis, and R.B. Bird. *Molecular Theory of Gases and Liquids*. New York City, New York: John Wiley and Sons. 1954.

Klavetter, E.A. and R.R. Peters. "Estimation of Hydrologic Properties of an Unsaturated, Fractured Rock Mass." SAND84–2642. Albuquerque, New Mexico: Sandia National Laboratories. 1986.

Liu, H.H., C. Doughty, and G.S. Bodvarsson. "An Active Fracture Model for Unsaturated Flow and Transport in Fractured Rock." *Water Resources Research*. Vol. 34, No. 10. pp. 2,633–2,646. 1998.

Mohanty, S., T.J. McCartin, and D. Esh. "Total-system Performance Assessment (TPA) Version 4.0 Code: Module Descriptions and User's Guide." San Antonio, Texas: CNWRA. 2002.

Mualem, Y. "A New Model for Predicting Hydraulic Conductivity of Unsaturated Porous Media." *Water Resources Research*. Vol. 12. pp. 513–522. 1976.

Painter, S.L., P.C. Lichtner, and M.S. Seth. "MULTIFLO User's Manual: Two-Phase Nonisothermal Coupled Thermal-Hydrologic-Chemical Flow Simulator." MULTIFLO Version 1.5. San Antonio, Texas: CNWRA. 2001.

Phillips, O.M. "Infiltration of a Liquid Finger Down a Fracture into Superheated Rock. *Water Resources Research*. Vol. 32, No. 6. pp. 1,665–1,670. 1996.

Pruess, K. and T.N. Narasimhan. "A Practical Method for Modeling Fluid and Heat Flow in Fractured Porous Media." *Society of Petroleum Engineers Journal*. Vol. 25, No. 1. pp. 14–26. 1985.

Somerton, W.H., A.H. El-Shaarani, and S.M. Mobarak. "High-Temperature Behavior of Rocks Associated with Geothermal Type Reservoirs." Proceedings of the Society of Petroleum Engineers 44th Annual California Regional Meeting. Paper SPE–4897. San Francisco, California: Society of Petroleum Engineers. 1974.

TRW Environmental Safety Systems, Inc. "Thermal Tests Thermal-Hydrological Analyses/Model Report." Las Vegas, Nevada: TRW Environmental Safety Systems, Inc. 2000.

———. "Thermal Test Progress Report #4." Las Vegas, Nevada: TRW Environmental Safety Systems, Inc. 1999a.

———. "Thermal Test Progress Report #3." Las Vegas, Nevada: TRW Environmental Safety Systems, Inc. 1999b.

———. "Thermal Test Progress Report #1." Las Vegas, Nevada: TRW Environmental Safety Systems, Inc. 1998a.

———. "Thermal Test Progress Report #2." Las Vegas, Nevada: TRW Environmental Safety Systems, Inc. 1998b.

———. "Drift-Scale Test As-Built Report." BAB00000–01717–5700–0003. Rev. 01. Las Vegas, Nevada: TRW Environmental Safety Systems, Inc. 1998c.

———. "Ambient Characterization of the Drift-Scale Test Block." BADD00000–01717–5705–00001. Rev. 01. Las Vegas, Nevada: TRW Environmental Safety Systems, Inc. 1997a.

———. "Drift-Scale Test Design and Forecast Results." B00000000–01717–4600–00007. Rev. 00. Las Vegas, Nevada: TRW Environmental Safety Systems, Inc. 1997b.

Tsang, Y.W. and J.T. Birkholzer. "Predictions and Observations of the Thermal-Hydrological Conditions in the Single Heater Test." *Journal of Contaminant Hydrology*. Vol. 38. pp. 385–425. 1999.

Tsang, Y.W., J. Apps, J.T. Birkholzer, B. Freifeld, M.Q. Hu, J. Peterson, E. Sonnenthal, and N. Spycher. "Yucca Mountain Single Heater Test Final Report." LBNL–42537. Berkeley, California: Lawrence Berkeley National Laboratory. 1999.

van der Kwaak, J.E., P.A. Forsyth, K.T.B. MacQuanie, and E.A. Sudicky. "WATSOLV, Sparse Matrix Iterative Solver Package, User's Guide." Waterloo, Ontario, Canada: Waterloo Centre for Groundwater Research, University of Waterloo. 1995.

van Genuchten, M.Th. "A Closed-Form Equation for Predicting the Hydraulic Conductivity of Unsaturated Soils." *Soil Science Society of American Journal*. Vol. 44. pp. 892–898. 1980.

Walton, J. and P. Lichtner. "Quasi-Steady State Model for Coupled Liquid, Vapor, and Heat Transport: Application to the Proposed Yucca Mountain High-Level Waste Repository." San Antonio, Texas: CNWRA. 1995.